SmdA is a novel cell morphology determinant in *Staphylococcus aureus*

Ine Storaker Myrbråten[1], Gro Anita Stamsås[1], Helena Chan[2,3], Danae Morales Angeles[1], Tiril Mathiesen Knutsen[1], Zhian Salehian[1], Volha Shapaval[4], Daniel Straume[1] and Morten Kjos[1].

[1] Faculty of Chemistry, Biotechnology and Food Science, Norwegian University of Life Sciences, Ås, Norway.

[2] Structural Cellular Biology Unit, Okinawa Institute of Science and Technology, Okinawa, Japan.

[3] The ithree institute, University of Technology Sydney, Broadway, NSW, Australia.

[4] Faculty of Science and Technology, Norwegian University of Life Sciences, Ås, Norway.

Abstract

Cell division and cell wall synthesis in staphylococci need to be precisely coordinated and controlled to allow the cell to multiply while maintaining their nearly spherical shape. The mechanisms ensuring correct placement of the division plane and synthesis of new cell wall have been studied intensively, however, hitherto unknown factors and proteins are likely to play key roles in this complex interplay. We here identified and investigated a protein with major influence on cell morphology in *Staphylococcus aureus*. The protein, named SmdA (for staphylococcal morphology determinant A), is a membrane-protein with septum-enriched localization. By CRISPRi knockdown and overexpression combined with different microscopy techniques, we demonstrate that proper levels of SmdA is necessary for cell division, including septum formation and cell splitting. We also identified conserved residues in SmdA that are critical for its functionality. Pulldown- and bacterial two-hybrid interaction experiments showed that SmdA interacts with several known cell division- and cell wall synthesis proteins, including penicillin binding proteins (PBPs) and EzrA. Notably, SmdA also affects susceptibility to cell wall targeting antibiotics, particularly in methicillin-resistant *S. aureus* (MRSA). Together, our results show that *S. aureus* is dependent on balanced amounts of membrane-attached SmdA in order to carry out proper cell division.

30 **Importance**

31 *Staphylococcus aureus* is an important human and animal pathogen. Antibiotic resistance is a
32 major problem in treatment of staphylococcal infections, and cell division and cell wall
33 synthesis factors have previously been shown to modulate susceptibility to antibiotics in this
34 species. In the current work we investigated the function of an essential protein named SmdA,
35 which was identified based on its septal localization and knockdown phenotype resulting in
36 defective cellular morphologies. We demonstrate that this protein is critical for normal cell
37 division in *S. aureus*. Depletion of SmdA sensitize resistant staphylococci to β-lactam
38 antibiotics. This work thus reveals a new staphylococcal cell division factor and a potential
39 future target for narrow spectrum antimicrobials or compounds to resensitize antibiotic
40 resistant staphylococcal strains.

41 ## Introduction

42 Most bacteria are surrounded by a shape-determining cell envelope which protects against lysis
43 and interacts with the extracellular milieu. The cell envelope of the opportunistic, Gram-
44 positive pathogen *Staphylococcus aureus* consists of a thick layer of peptidoglycan (PG) along
45 with teichoic acids (TA) and cell wall-associated surface proteins. During a bacterial cell cycle,
46 synthesis of PG and TA needs to be precisely regulated and coordinated with cell division,
47 DNA replication and chromosome segregation. Tight control of these processes is critical for
48 staphylococcal cells to maintain their integrity and nearly spherical shape as they multiply, and
49 they are therefore attractive targets for antimicrobials (1). Exactly how such control is mediated
50 in *S. aureus* is still not fully established, and hitherto unknown factors may be involved. In this
51 work we describe a new staphylococcal cell morphology determinant.

52 Staphylococcal cell division is initiated by assembly of the Z-ring, consisting of
53 polymerized FtsZ-proteins, that localizes to the future division septa (2). The Z-ring functions
54 as a scaffold for cell division- and cell wall synthesis proteins which together constitute the
55 divisome (3). Cell division in *S. aureus* occurs in alternating orthogonal planes, meaning that
56 the new cell division plane is always perpendicular to the previous (4). Timely and spatial
57 control of localization of the Z-ring assembly is most likely linked with chromosome
58 segregation and DNA replication, involving proteins such as the nucleoid occlusion factor Noc,
59 which ensures that the cells do not establish new septa across the chromosomes (5), and CcrZ,
60 which connects initiation of DNA replication to cell division (6). The chromosomes and
61 chromosome segregation also contribute to establish a physical barrier allowing the Z-ring only
62 to be formed in an angle perpendicular to the previous division plane (4).

63 The Z-ring directs the synthesis of new PG in *S. aureus* to the septum. Synthesis of PG
64 starts in the cytoplasm, where UDP-MurNAc-pentapeptide is first synthesized and then
65 attached to the membrane by the enzyme MraY to form the PG precursor lipid I (7, 8). A

66 GlcNAc residue and a pentaglycine side chain is attached to produce lipid II-Gly_5 (9), which
67 is flipped to the outer leaflet of the membrane by MurJ (10, 11) where it is incorporated into
68 the existing PG mesh by transpeptidation (TP) and transglycosylation (TG) reactions.
69 Specifically, the shape, elongation, division and sporulation (SEDS) proteins, FtsW and RodA
70 with TG activity, work in pairs with monofunctional transpeptidases, the penicillin binding
71 proteins PBP1 and PBP3, respectively (12, 13). While the PBP1-FtsW pair is essential and
72 performs the septal cross wall synthesis, the non-essential PBP3-RodA pair is responsible for
73 the slight elongation taking place in *S. aureus*. Additionally, *S. aureus* possesses two other
74 PBPs; the bifunctional PBP2 with both TG and TP activity, whose role is essential in *S. aureus*,
75 and the low-molecular weight PBP4, which controls the degree of PG crosslinks (14-16).
76 Finally, MRSA strains have an additional PBP, PBP2A, a transpeptidase with low-affinity for
77 β-lactam antibiotics (17, 18). In the final step of division, PG hydrolases break covalent bonds
78 in PG for cell wall remodeling and daughter cell splitting. The major, bifunctional autolysin
79 Atl, together with Sle1, for which expression are regulated by the two-component system
80 WalKR, are the primary enzymes responsible for hydrolyzing the septal PG to allow splitting
81 of daughter cells (19-22). The actual cross wall splitting is a mechanical process occurring
82 within milliseconds (23, 24).

83 The spatiotemporal control of cell division and PG synthesis is directly and indirectly
84 influenced by several factors. One of these is the anionic TA polymers, the second major
85 component of the cell wall, which are either covalently linked to the PG (wall teichoic acids,
86 WTA), or linked via a lipid-anchor to the plasma membrane (lipoteichoic acids, LTA).
87 Mutations in enzymes involved in either WTA or LTA biosynthesis result in cells of abnormal
88 shape and lack of septum synthesis control, probably via different mechanisms (15, 25, 26).
89 Furthermore, proteases, chaperones and secretion proteins, involved in production, folding
90 and/or secretion of cell cycle proteins, may also directly or indirectly affect coordination of cell

division and septum formation in *S. aureus*. For example, Clp-protease complexes can target both FtsZ and Sle1, and thereby have major effects on these processes (27-29).

Evidently, cell shape maintenance and control of cell division and septum formation are a complex interplay between many cellular processes where unknown key factors are yet to be discovered. We here identified a hitherto novel protein named SmdA (for staphylococcal morphology determinant A). We show that the level of the membrane-attached SmdA protein is critical for maintaining normal division progression and morphology in *S. aureus*, as silencing or overexpression of *smdA* resulted in defective cell division and septal cross wall synthesis, as well as increased sensitivity towards cell wall targeting antibiotics.

Results

SmdA is a conserved staphylococcal membrane protein

To identify novel proteins potentially involved in cell cycle and morphology control in *S. aureus*, we performed a combined depletion- and subcellular localization analysis of essential staphylococcal proteins with no annotated functions (30-32). From this, we identified a septum-enriched protein (SAOUHSC_01908, named SmdA), whose knockdown resulted in cells of variable sizes that formed large clusters (see below). The function of SmdA in *S. aureus* was investigated further here.

SmdA is a protein of 302 amino acids which is fully conserved in species within the *Staphylococcaceae* family (Fig. S1). The *smdA* gene is monocistronic and located >100 bp away from the neighboring genes (SAOUHSC_01907; unknown function, and *metK*; S-adenosylmethionine synthase). The protein has a predicted N-terminal transmembrane helix and a C-terminal cytoplasmic part with partial homology to a so-called nuclease related domain (NERD) (PF08375, $E = 1.08 \cdot 10^{-5}$) (Fig. 1A). The domain was named based on distant similarities to endonucleases, and is found in bacterial, archaeal, as well as plant proteins (33).

116 However, the functional role of NERD in bacteria has to our knowledge never been studied.
117 SmdA has been found to be essential in transposon mutagenesis studies in *S. aureus* (30, 32).
118 Growth analysis of SmdA CRISPRi knockdown (hereafter $SmdA^{down}$) in *S. aureus* SH1000 in
119 rich medium at 37°C resulted in a reduction in growth compared to the control strain when
120 spotted on agar plates (Fig. 1B). The growth rate in liquid medium was only slightly affected
121 when CFU and OD_{600} was determined at different time points in the same culture during growth
122 (Fig. S2A). By RT-PCR we verified that the expression of *smdA* was indeed fully knocked
123 down by the CRISPRi system in *S. aureus* SH1000 (Fig. S2B). Since the $SmdA^{down}$ strains
124 were still viable, we attempted to construct deletion mutants of *smdA* by allelic replacement
125 with a spectinomycin resistance cassette using the pMAD-vector (34). However, we were not
126 able to obtain the deletion mutant in *S. aureus* SH1000. Similarly, for *S. aureus* strains
127 NCTC8325-4, HG001 and the MRSA strain COL, $SmdA^{down}$ resulted in reduced growth on
128 agar plates, with HG001 being most affected (Fig. 1B), but we were not able to obtain any
129 deletion mutants in these strains. We therefore used the CRISPRi system in the different *S.*
130 *aureus* strains to study the phenotypes of SmdA further.
131
132 **Depletion and overexpression of SmdA result in cells with highly aberrant cell shapes**
133 During the initial analysis, we observed that $SmdA^{down}$ in *S. aureus* SH1000 resulted in clusters
134 containing cells of variable sizes. The knockdown experiment was repeated, and exponentially
135 growing cells were stained with fluorescent vancomycin (VanFL, binds to non-crosslinked
136 stem peptides throughout the cell wall). $SmdA^{down}$ indeed resulted in severe phenotypic defects
137 (Fig. 1C); increased cell clustering and a large fraction of cells with multiple septa (20.1 % for
138 $SmdA^{down}$ as opposed to 1.6 % for the control strain, Fig. 1D) and abnormal, non-spherical
139 morphology (Fig. 1E). The $SmdA^{down}$ cells were also significantly larger than the control strain
140 (Fig. 1F).

141 Transmission- and scanning electron microscopy (TEM and SEM) were used to obtain
142 more detailed images of the defects in morphology and septal placement found in SmdA^{down}
143 cells. Strikingly, SmdA depleted *S. aureus* SH1000 displayed highly aberrant septum formation
144 (Fig. 2A). In addition to lysis, cells with several non-perpendicular- or parallel septa were
145 frequently observed, resulting in cells, or small cell clusters, with aberrant morphologies (Fig.
146 2A). This was also evident from the SEM micrographs, which showed clustered cells with
147 various morphologies (Fig. 2B). Similar phenotypes from TEM and SEM analyses were
148 observed for the NCTC8325-4, HG001 and COL strains, with the HG001 strain being more
149 affected by SmdA^{down} than the other two (Fig. S3 and Fig. S4).

150 Since reduced levels of SmdA led to defects in cell division and morphology of *S.*
151 *aureus*, we next wondered whether overexpression of SmdA would affect the cells. An ectopic
152 copy of *smdA* under control of an IPTG-inducible promotor in the plasmid pLOW (35) was
153 expressed in *S. aureus* NCTC8325-4. As for SmdA^{down}, the cells were stained with VanFL (Fig.
154 S5A). Although less evident than for SmdA^{down}, overexpression of SmdA also resulted in
155 clusters of cells with several septa per cell as defined by VanFL staining (Fig. S5A) (3.9 %, n
156 = 181 for SmdA overexpression, compared to 20.1 % for SmdA^{down}, and 1.6 % for the control).
157 Together, these knockdown- and overexpression experiments clearly demonstrate that septum
158 formation and splitting in *S. aureus* are dependent on proper levels of SmdA.

159

160 **Depletion of SmdA results in increased sensitivity towards antimicrobials targeting cell**
161 **wall synthesis**

162 Given the negative effect SmdA depletion had on cell morphology and -division, we reasoned
163 that reduced expression of SmdA could influence the sensitivity of *S. aureus* to cell wall
164 targeting antibiotics. To test this, SmdA^{down} strains were treated with PBP-targeting β-lactams
165 (oxacillin, cefotaxime, cefoxitin and imipenem), the glycopeptide vancomycin (blocking cell

166 wall synthesis by targeting the terminal D-Ala-D-Ala on the stem peptides of nascent PG (36)),
167 tunicamycin (targeting TarO and MraY, enzymes involved in the early stages of WTA and PG
168 synthesis, respectively (37)), targocil (targeting the WTA exporter TarG (38)) and Congo Red
169 (inhibitor of the LTA biosynthesis enzyme LtaS (39)) (Table 1). Two antibiotics with
170 alternative targets; tetracycline (targeting protein synthesis) and ciprofloxacin (a quinolone
171 targeting DNA synthesis), were also included.

172 For the methicillin-susceptible *S. aureus* (MSSA) strain SH1000, a two-fold reduction
173 in minimum inhibitory concentration (MIC), compared to the control, was observed for
174 oxacillin and cefoxitin in SmdA^{down}. More notably, in the MRSA strain COL, SmdA^{down}
175 sensitized the COL strain towards all β-lactams with a 2- to 8-fold reduction in MIC compared
176 to the control (Table 1). SmdA depletion did not seem to significantly influence vancomycin
177 susceptibility. Strikingly, however, we observed that SmdA^{down} cells became highly sensitive
178 towards tunicamycin, with a 64-fold reduction in MIC compared to the control for *S. aureus*
179 SH1000 and >4-fold reduction for COL (40, 41). We therefore also tested the tunicamycin
180 sensitivity of the NCTC8325-4 and HG001 SmdA^{down} strains, which also showed increased
181 susceptibility towards tunicamycin (HG001; 125-fold reduced MIC and NCTC8325-4; 4-fold
182 reduced). While no difference in MIC was observed for targocil, the SmdA^{down} strains also
183 displayed increased sensitivity towards Congo Red. Finally, SmdA depletion in *S. aureus*
184 SH1000 led to a 2- to 4-fold reduction in MIC against tetracycline, compared to the control,
185 however, depletion of SmdA in COL did not change its sensitivity towards tetracycline or
186 ciprofloxacin (Table 1).

187

188 **SmdA has no major effects on the TA biosynthetic pathways**

189 The increased sensitivity to tunicamycin and Congo Red in SmdA^{down} strains, prompted us to
190 study whether there were any major alterations in the TA in these cells, although it was also

191 noted that no changes in sensitivity was observed for the WTA export inhibitor targocil (Table
192 1). Notably, the SmdA^{down} strain displayed morphologies reminiscent of what has previously
193 been reported for cells depleted of TA, i.e., with larger cell sizes, cells with irregular septum
194 formations and reduced splitting (26, 37, 38, 42). It has previously been shown that there is a
195 synthetic lethal relationship between the WTA and LTA biosynthetic pathways (42, 43), and it
196 could therefore be hypothesized that hypersensitivity to tunicamycin could result from deficient
197 LTA biosynthesis in the *smdA^{down}* mutants, Using an anti-LTA antibody, we compared the
198 quantity and lengths of LTA in the SmdA^{down} - and control strains for SH1000, NCTC8325-4,
199 HG001 and COL (Fig. S6A). For HG001, the strain with most severe division defects, we
200 observed a reduction in LTA amounts in SmdA^{down} and this can possibly contribute to the
201 severe phenotype of this strain. However, no consistent changes in LTA amounts or lengths
202 were observed between the SmdA depletions and the controls in the four strains. Furthermore,
203 we could not detect any LTA release into the growth medium in the depletion strains, indicating
204 that the stability of LTA (44) was intact (Fig. S6B). We therefore conclude that SmdA does
205 not have any consistent effect on LTA synthesis across strains.

206 WTA has been shown to protect cells from the LTA-inhibitor Congo Red. Without
207 WTA, cells became hypersensitive towards Congo Red (MIC of <4 µg/ml for *tarO* deletion
208 mutants and >1024 µg/ml for wild-type cells) (45). Although to a much lesser degree, SmdA
209 depletion strains were also more sensitive to Congo Red compared to the controls (Table 1),
210 and we therefore looked into whether WTA could be disturbed in a SmdA^{down} strain. Cells
211 without WTA has previously been shown to lack the dark, electron-dense layer observed in
212 TEM images of crosswalls of *S. aureus* wild type cells (Fig. S6C) (37, 46). TEM images of
213 TarO^{down} and SmdA^{down} showed that TarO^{down}, as expected (37, 46), lacked this dark, high-
214 density layer, while it was still present in the SmdA^{down} strain, suggesting that WTA was still
215 produced (Fig. S6C). We also performed Fourier transform infrared spectroscopy (FTIR),

216 which has been used before to detect differences in the composition of WTA due to variable
217 glycosylation patterns (44, 47). As expected, changes in the FTIR spectra were evident in the
218 polysaccharide region (1200 cm^{-1} - 800 cm^{-1}) for the $TarO^{down}$ strain compared to the control,
219 with the most significant differences recorded for the peaks at 1076 cm^{-1}, 1048 cm^{-1}, 1033 cm^{-}
220 ^{1} and 1000 - 970 cm^{-1}, representing α- and β-glycosidic bonds in WTA (47). However, no
221 changes were observed between $SmdA^{down}$ and the control (Fig. S6D). Together, these results
222 suggests that SmdA has no major effect on the WTA biosynthetic pathway.
223

224 **SmdA is important in several stages of staphylococcal cell division**

225 To identify potential protein interaction partners of SmdA, we next performed a protein
226 pulldown experiment using GFP-trapping with a chromosomal *smdA-m(sf)gfp* fusion strain.
227 Interestingly, the major staphylococcal autolysin Atl, as well as the bifunctional PBP2 were
228 identified, along with 12 other proteins (Table S1). The experiment was repeated in a strain
229 with plasmid-based expression of SmdA-m(sf)GFP, and this setup resulted in an extended list
230 of proteins that were pulled down, probably due to the elevated expression of SmdA-m(sf)GFP.
231 Selecting the proteins for which at least 10 unique peptides were detected and with a fold
232 change of >2 compared to the control, resulted in a list of 57 proteins (Table S1). Several
233 proteins with activity involved in protein folding, secretion and/or degradation (e.g., FtsH,
234 PrsA, SpsB, ClpB, ClpC, SecD) were identified in this assay, in addition to the penicillin-
235 binding proteins PBP1, PBP2, PBP3 and the early division protein EzrA. All the 14 proteins
236 identified in the initial experiment were also pulled down in the second experiment.

237 Bacterial two-hybrid analyses of the SmdA-PBP1-3 and SmdA-EzrA were performed
238 to see whether these interactions could be reproduced in a heterologous system. The proteins
239 were fused either N- or C-terminally to the domains of adenylate cyclase, an enzyme which
240 catalyzes the production of cyclic adenosine monophosphate (cAMP) and eventually induction

241 of β-galactosidase production when brought in proximity by interaction between the target
242 proteins. Indeed, SmdA interacted with PBP2, as well as PBP1, PBP3 and EzrA in the two-
243 hybrid assays (Fig. 3A). By expressing a version of SmdA without its N-terminal membrane
244 domain (SmdAΔTMH), we also show that the observed interactions between SmdA and the
245 PBPs in this assay occur via the transmembrane segment, while the interaction with EzrA was
246 retained for SmdAΔTMH. The latter suggests that EzrA interacts with the intracellular part of
247 SmdA (Fig. 1A). Furthermore, we also show that SmdA is able to self-interact, and also this
248 interaction is dependent on the transmembrane helix (Fig. S7).

249 The observed interactions between SmdA and PBPs may suggest that SmdA is
250 somehow important for proper regulation and/or localization of PBPs in *S. aureus* (Fig. 1 and
251 Fig. 2). The VanFL approach used above (Fig. 1C) labels non-crosslinked PG throughout the
252 cell surface. Therefore, to determine more precisely the sites of active PG synthesis in *S. aureus*
253 NCTC8325-4 SmdA^{down} and SmdA overexpression cells, we pulse-labelled the cells for 90 sec
254 with the fluorescent D-amino acid 7-hydroxycoumarincarbonylamino-D-alanine (HADA), a
255 molecule which is integrated into PG by the specific activity of transpeptidases (48). In the
256 control cells, the expected midcell-localized band was observed (Fig. 3B). However, in the
257 SmdA^{down} strain, we observed a more diffuse HADA signal with PG synthesis often occurring
258 at several sites within the cell, forming patterns visible as crosses or Y-shapes (Fig. 3C). Similar
259 observations were made in the cells overexpressing SmdA, although with a lower frequency
260 (Fig. 3D-E). Thus, the site of active transpeptidation (and thus probably at least one of the
261 PBPs) is mis-localized when the levels of SmdA is altered.

262 Moreover, we also studied whether SmdA could affect the localization of EzrA by
263 knocking down *smdA* in a strain expressing a chromosomal *ezrA-gfp* fusion (Fig. 3F). Indeed,
264 abnormal localization patterns for EzrA-GFP was observed with similar frequency as the
265 abnormal HADA labelling (Fig. 3G). These results thus suggest that depletion of SmdA,

266 directly or indirectly, influences the localization of both early and late divisome proteins in *S.*
267 *aureus*.

268 Furthermore, the major autolysin Atl was also pulled down with SmdA. Atl is a secreted
269 multidomain enzyme, which is processed to an acetylmuramyl-L-alanine amidase and β-N-
270 acetylglucosaminidase, involved in septal cross wall splitting resulting in daughter cell
271 separation (19). SmdA^{down} cells frequently displayed increased clustering (Fig. 2, Fig. S4). This
272 indicates reduced cross wall splitting, a phenotype also observed in Δ*atl* mutants and WalKR
273 depleted cells (22, 49). WalKR is the two-component regulatory system controlling the
274 expression of *atl* and other cell wall hydrolase encoding genes (22). To assess the reduced cross
275 wall splitting phenotype in more detail, we performed Triton X-100-induced autolysis assays
276 on the cultures. Indeed, reduced autolysis was observed in SmdA^{down} cells, demonstrating
277 reduced autolytic activity (Fig. 4A). The lysostaphin sensitivity was also reduced (Fig. 4B),
278 suggesting alterations in the cell wall affecting the lytic properties of this enzyme. It should be
279 noted that the resistance towards Triton X-100- and lysostaphin-induced autolysis in the
280 SmdA^{down} strain was clearly less compared to the control strain where *walR*, and thus all the
281 regulated autolysins, was knocked down. It should also be noted that Triton-X induced
282 autolysis was not severely altered upon overexpression of SmdA (Fig. S5B).

283

284 **SmdA localizes at the septal region after FtsZ**

285 The SmdA-m(sf)GFP fusion protein displayed a septum-enriched signal when expressed
286 ectopically from the low copy-number plasmid pLOW (Fig. 5A). In order to analyze the SmdA
287 localization with native expression levels, a chromosomally integrated version of *smdA-*
288 *m(sf)gfp* was made, in which SmdA was expressed with m(sf)GFP fused to its C-terminus.
289 Localization analyses in these cells further confirmed the septum-enriched localization of the
290 fusion protein (Fig. 5A), with an average septum/periphery fluorescence signal ratio of 3.4 (n

291 = 52, see Materials and Methods). To visualize the localization of SmdA relative to the cell
292 division process, we used FtsZ as a marker. Expression of *ftsZ*-fusion genes in the *smdA-*
293 *m(sf)gfp* chromosomal fusion strain, however, only resulted in strains with extremely poor
294 growth, suggesting that the cells did not tolerate such double-labelling. Instead, we therefore
295 created a double-labelled strain in which SmdA-mYFP and FtsZ-mKate2 were co-expressed
296 from plasmids, while the native *smdA* and *ftsZ* genes were still present on the chromosome.
297 Structured illumination microscopy (SIM) analysis showed that SmdA-mYFP is localized
298 around in the membrane when the Z-ring is formed (Fig. 5B), and that a septum-enriched
299 localization occurs as the septal cross wall is being synthesized. This was further confirmed by
300 stimulated emission depletion (STED) microscopy analysis (Fig. 5C). STED imaging also
301 revealed that there was no apparent co-localization of SmdA-mYFP and FtsZ-mKate2 in
302 newborn cells before FtsZ-constriction initiates. Combined, the localization of SmdA is
303 reminiscent of the localization of PBPs in *S. aureus* (11), but appears to localize to the septal
304 area after the early divisome proteins such as EzrA (50, 51).

305 The SmdA protein is anchored to the membrane by a single transmembrane helix (Fig.
306 1A). To verify its significance for the septal localization, we ectopically expressed a version of
307 SmdA without the transmembrane helix (SmdAΔTMH). The N-terminally truncated
308 SmdAΔTMH-m(sf)GFP localized to the cytoplasm of the cells (Fig. 5A). This shows that while
309 the transmembrane helix is critical for protein-protein interactions and subcellular localization
310 of SmdA, the interaction observed between EzrA and SmdAΔTMH (and full-length SmdA)
311 (Fig. 3A) is probably not involved in determining the localization of this protein.

312 During these latter experiments, we noticed that SmdAΔTMH-m(sf)GFP
313 overexpression led to cells with obvious morphology defects. In fact, overexpression of
314 SmdAΔTMH (without the GFP-tag) (Fig. 6A) strikingly resulted in a more extreme phenotype
315 than overexpression of full length SmdA (Fig. 3D, Fig. S5). The cells were often inflated or

316 with a bean-shaped appearance (Fig. 6A). HADA pulse labelling of these cells revealed a
317 highly abnormal PG incorporation pattern, with the fluorescent signal forming both condensed
318 clumps and Y-shapes in different directions in almost 50 % of the cells (Fig. 6A and B). This
319 demonstrates that membrane attachment is critical for the localization and function of SmdA.
320

321 **Conserved amino acids in the predicted NERD domain are critical for the function of**
322 **SmdA**

323 The functional importance of the NERD domain (Fig. 1A) has, to our knowledge, neither been
324 studied nor verified previously in any bacterial protein. As mentioned, we observed that
325 overexpression of SmdAΔTMH led to severe phenotypic changes in the staphylococcal
326 morphology (Fig. 6A). We decided to use this as a tool to gain insight into whether the
327 predicted NERD domain is important for the function of SmdA. Multiple sequence alignment
328 of SmdA proteins from different staphylococcal species (Fig. S1) revealed conserved residues
329 in this domain, and site directed mutagenesis was used to create two versions of SmdAΔTMH
330 containing mutations in the NERD domain: one in which H145 was changed to Ala (mut1),
331 and a second containing the mutations R150A and T151A (mut2). Furthermore, we also
332 observed from the alignment that the C-terminus of SmdA is highly conserved (Fig. S1), and
333 another C-terminally mutated variant was created (mut3; F280A, H281A). The three-
334 dimensional structure of SmdA, predicted by AlphaFold (52), suggests that the N-terminal part
335 of the protein folds into a long α-helix and that the NERD domain is located within the C-
336 terminal structured part of the protein (Fig. 6C-II). The mutated SmdAΔTMH versions were
337 overexpressed in a wild-type background. Expression of these mutated variants indeed
338 partially, or fully, abolished the phenotypic defects observed when overexpressing the non-
339 mutated SmdAΔTMH version. HADA staining of mut1 (H145A) showed septum placement
340 and PG synthesis comparable to wild-type cells, while mut2 (R150A, T151A) and mut3

341 (F280A, H281A) also clearly reduced the functionality of the protein (Fig. 6A and B).
342 Furthermore, the growth inhibition upon overexpression of SmdAΔTMH (Fig. 6D) was also
343 abolished when the mutated variants were expressed under the same conditions. This strongly
344 suggests that the given residues in both the predicted NERD and the conserved C-terminus are
345 important for the function of SmdA.
346

347 **Discussion**

348 The results presented here provide the first functional insights into the conserved
349 staphylococcal protein SAOUHSC_01908, here named SmdA. SmdA, a protein conserved
350 within the *Staphylococcaceae* family, is critical for maintaining cell morphology and for proper
351 progression of cell division in different *S. aureus* strains (including MRSA and MSSA).
352 Unbalanced levels, as well as loss of proper subcellular localization, of SmdA, result in severe
353 cell morphology defects due to mis-localized cell division, uncontrolled cell wall synthesis,
354 and lack of proper cross wall splitting.

355 We observed that knockdown of SmdA increased the sensitivity of *S. aureus* to several
356 cell wall targeting antibiotics, including β-lactams and tunicamycin (Table 1). Many of the
357 frequently used antibiotics, including β-lactams, target cell wall synthesis, but the rise of both
358 methicillin- resistant- and vancomycin-resistant *S. aureus* (MRSA and VRSA) have made *S.*
359 *aureus* infections more difficult to treat and novel anti-staphylococcal targets and strategies are
360 needed. Targeting cell cycle proteins have been shown to re-sensitize resistant staphylococci
361 towards existing antibiotics due to synergistic effects (53-55). For example, inactivation of
362 some proteins involved in WTA synthesis sensitizes MRSA to β-lactams (37, 56). The same is
363 also the case for a diversity of factors contributing to cell division and cell wall biogenesis,
364 including FtsZ, FtsA, PBP4 and most proteins involved in the PG synthesis pathway (55). The
365 secretion-associated proteins SecDF and the chaperones PrsA and HtrA1 have also been tightly

366 linked to β-lactam sensitivity (57, 58), and recently, inactivation of the autolytic cell wall
367 amidase Sle1 (21), or the membrane proteins AuxA and AuxB (44), were shown to result in
368 increased sensitivity to β-lactams. Mechanisms of re-sensitization in these cases vary and may
369 be a result of weakened cell wall, as well as inactivation or mis-localization of PG synthesis,
370 including the key resistance determinant PBP2A. The large number of factors affecting β-
371 lactam sensitivity reflects the tight links between different processes involved in cell wall
372 biosynthesis, and most likely SmdA affects several steps in the cell division process (Fig. 1-3).

373 The exact mechanism by which SmdA affects these processes remains to be determined.
374 Our results suggest that cell division and PG synthesis, but not teichoic acid biosynthesis, is
375 affected. This is supported by observations showing mis-localization of cell division and PG
376 synthesis in SmdA^{down} cells (Fig. 1-3). Furthermore, SmdA^{down} cells displayed hypersensitivity
377 towards tunicamycin (targeting enzymes involved both in PG and WTA synthesis), but not
378 towards targocil (targeting the WTA exporter only) (38). Possibly, SmdA influences the
379 localization of cell division and cell wall synthesis by direct protein-protein interactions. This
380 is supported by the SmdA-EzrA and SmdA-PBP1-3 interactions, combined with the abnormal
381 localization of EzrA-GFP and HADA incorporation in SmdA^{down} cells (Fig. 3). In fact, the
382 division defects observed in SmdA^{down} cells (Fig. 1-3) are reminiscent of previous studies of
383 *ezrA* null mutants, strains with point mutations in FtsZ or cells exposed to Z-ring inhibitors (50,
384 51, 59, 60). However, the contribution of the identified interactions to the observed phenotypes
385 must be investigated further, particularly since the subcellular localization of SmdA-m(sf)GFP
386 does not appear to overlap with the Z-ring throughout the cell cycle. The SmdA-localization,
387 which depends on the transmembrane helix, is instead more similar to the reported localization
388 of PBPs (Fig. 5) (11, 50, 51).

389 Lack of cross wall splitting is another prominent feature of the SmdA depleted cells
390 (Fig. 2 and 4). After septum formation, cells remain attached, forming clusters of mis-shaped

391 cells. Indeed, the autolytic activity was reduced in the SmdA^{down} cells (Fig. 4). The major
392 autolysin Atl was also pulled down together with SmdA-m(sf)GFP as one of the major hits
393 (Table S1). Atl is an extracellular processed protein whose amidase and glucosaminidase
394 domains together process PG in the septum to allow splitting. It is possible that SmdA
395 somehow influences the export or processing of Atl. In this context, it is interesting to note that
396 proteases, foldases and chaperones (FtsH, PrsA, SpsB, ClpC, ClpB, HtrA1) were also pulled
397 down with SmdA (Table S1). It remains to be determined whether these interactions have any
398 functional relevance, however, perturbation of such pathways may have major consequences
399 for cell division and septal placement as they are important for proper folding and secretion of
400 key proteins involved in such processes. This has, for example, previously been demonstrated
401 for the chaperone ClpX, which is critical for coordination of autolysins and cell division
402 proteins (29). Involvement in such a mechanism could also explain the pleiotropic phenotypes
403 observed in SmdA^{down} cells, affecting several stages in the cell division process.

404 A part of SmdA displays limited similarity to the so-called nuclease related domain
405 (NERD). This domain, which is found in a broad range of bacterial species and in some archaea
406 and plants, was initially identified on a virulence-plasmid from *Bacillus anthracis* (33), and
407 has later been suggested to belong to a superfamily of phosphodiesterases (61). The majority
408 of NERD proteins are single-domain proteins, but they are also occasionally found together
409 with a kinase-, pseudokinase- or helicase domain (62). The actual function of the NERD has,
410 to our knowledge, however, not been studied experimentally. The results in this paper show
411 that conserved residues in the predicted NERD are important for the functionality of SmdA,
412 thus demonstrating for the first time a functional role of this domain (Fig. 6). Although highly
413 speculative at this point, it would be interesting if a cell division factor such as SmdA had
414 DNA-interacting capabilities and thus forming a potential link between the membrane-
415 associated cell division proteins and the nucleoid. It should also be noted that several of the

416 most conserved residues of the NERD domain (33) are not found in SmdA, suggesting a
417 functional diversity among proteins harboring homology to this domain and implying that the
418 NERD of SmdA may have functions unrelated to the nucleoid.

419 It is also interesting to note that the effect of SmdA knockdown was different between
420 strains. For example, SmdA^{down} resulted in a more severe phenotype in HG001 compared to
421 NCTC8325-4 and SH1000 (Fig. 1, Fig. S3-S4), although these strains derive from the same
422 parent (63). While HG001 contains prophages, NCTC8325-4 and SH1000 have been cured of
423 these, and it could for example be speculated that the stress imposed by knockdown of SmdA
424 somehow results in prophage induction in HG001 and thereby a more severe phenotype.
425 Understanding of these and other strain differences could also help to further pinpoint the exact
426 function of SmdA.

427 The staphylococcal genome encodes hundreds of essential proteins, which all represent
428 potential target sites for antimicrobials. To be able to fully exploit the antibiotic target
429 repertoire, it is critical to understand how essential proteins are involved and linked between
430 different cell cycle processes. In this work, we identified and characterized SmdA as a novel
431 factor essential for cell morphology and cell division in *S. aureus*. Based on the results
432 presented here, future research should aim at pinpointing the molecular mechanism by which
433 SmdA affect different stages of the cell division process. Finally, since SmdA depletion results
434 in increased sensitivity to β-lactams, it may as such also be a possible future target for
435 combatting β-lactam resistance by re-sensitizing MRSA to these antibiotics.

436

437 Materials and Methods

438 Bacterial strains, growth conditions and transformations

439 *Escherichia coli* IM08B (64), *E. coli* XL1-Blue and *E. coli* BTH101 were grown in lysogeny
440 broth (LB) at 30-37°C with shaking or on lysogeny agar (LA) plates at 30-37°C, with 100

441 µg/ml ampicillin and/or 50 µg/ml kanamycin for selection. *S. aureus* SH1000, NCTC8325-4,
442 HG001 and COL were grown in brain-heart infusion (BHI) broth or tryptic soy broth (TSB) at
443 37°C with shaking or on BHI/TSA plates at 37°C. For selection, 10 µg/ml of chloramphenicol,
444 5 µg/ml of erythromycin, 15 µg/ml neomycin or 100 µg/ml spectinomycin were added. For
445 induction of gene expression, 50 or 300 µM isopropyl β-D-1-thiogalactopyranoside (IPTG) or
446 2.5 ng/ml anhydrotetracycline (ATc) were added to the bacterial cultures.

447 A standard heat shock protocol was used for transformation of *E. coli* IM08B. Isolated
448 plasmids from *E. coli* were transformed into *S. aureus* by electroporation. Preparation of
449 electrocompetent *S. aureus* cells and electroporation were performed according to Löfblom et
450 al (65). Bacterial strains used in this study are listed in Table S2.

451

452 **Genetic modifications**

453 For all cloning, DNA fragments were amplified from *S. aureus* SH1000 genomic DNA, and
454 cloning was performed with restriction digestion (New England Biolabs [NEB]) and
455 subsequent ligation using T4 DNA Ligase (NEB), unless otherwise stated. Ligation mixtures
456 were transformed into *E. coli* IM08B, and sequence-verified plasmids were transformed into
457 *S. aureus.* All strains and primers used in this study are listed in Table S2 and Table S3,
458 respectively.

459

460 **Fluorescent fusion constructs**

461 *Construction of pLOW-smdA-m(sf)gfp.* Monomeric superfolder GFP, *m(sf)gfp*, was initially
462 fused to *ftsZ* in the plasmid pLOW (35). *m(sf)gfp* was amplified from the plasmid pMK17 (66)
463 using forward primer im1_linker_FP_F_BamHI (annealing to the linker sequence) and reverse
464 primer im2_m(sf)gfp_R_NotI_EcoRI. The amplified fragment encodes a linker sequence N-
465 terminally of the *m(sf)gfp* gene. The fragment was digested with BamHI and EcoRI and

466 subsequently ligated into the corresponding sites of the plasmid pLOW-*ftsZ-gfp* to replace the
467 original *gfp*-gene with the linker_m(sf)gfp sequence. SAOUSHSC_01908 was then amplified
468 with primers im77_SA1908_F_SalI_RBS and im78_SA1908_R_BamHI, the product was
469 digested with SalI and BamHI and ligated into the corresponding sites of pLOW-*ftsZ-m(sf)gfp*
470 to create pLOW-*smdA-m(sf)gfp*.
471
472 <u>*Construction of pMAD-smdA-m(sf)gfp_aad9 for chromosomal integration.*</u> To tag the
473 chromosomal *smdA*, the plasmid pMAD-*smdA-flag_aad9* was constructed initially. The insert
474 in this plasmid (*smdA-flag_aad9*) was assembled by overlap extension PCR (primers im147-
475 im152), with the flag-tag sequence inserted by primer overhangs, and cloned into pMAD (34)
476 using restriction enzymes MluI and BamHI and T4 DNA Ligase (NEB). The insert was
477 designed so that the flag-tag could be removed using NotI and SpeI. The *m(sf)gfp* sequence
478 was amplified from template pMK17 (66) using the primers im153 and im154. The PCR
479 product was digested with NotI and SpeI and subsequently ligated with NotI- and SpeI-digested
480 pMAD-*smdA-flag_aad9*. The ligation mix was transformed to *E. coli* IM08B, and the resulting
481 plasmid, pMAD-*smdA-m(sf)gfp_aad9,* was verified by sequencing and transformed into
482 electrocompetent *S. aureus* SH1000. Integration of *smdA-m(sf)gfp* in the native locus of *smdA*
483 using the temperature-sensitive pMAD-system was carried out as previously described (34).
484
485 <u>*Construction of pHC-ftsZ-mKate2*</u>. *ftsZ-mKate2* was amplified from the plasmid pLOW-*ftsZ-*
486 *mKate2*. pLOW-*ftsZ-mKate2* was made in a similar manner as described for pLOW-*ftsZ-*
487 *m(sf)gfp*, but with reverse primer im5_mKate_R_NotI_EcoRI and genomic DNA derived from
488 strain MK119 (67) as template for amplification of *mKate2*. Then, *ftsZ-mKate2* was amplified
489 with primers USHC109 and USHC148, generating a product with SalI and MluI as overhang.

490 The PCR product and the plasmid pSK9065 (68) were digested with SalI and MluI and
491 thereafter ligated.
492
493 *Construction of pLOW-smdA-mYFP*. This plasmid was constructed by using pLOW-*ftsZ-*
494 *mYFP* as starting point, made similarly as described for pLOW-*ftsZ-m(sf)gfp*, but with reverse
495 primer im3_cfp_myfp_R_NotI_EcoRI and plasmid pMK20 (lab collection) as template for
496 amplifying *mYFP*. The plasmids pLOW-*smdA-m(sf)gfp* (described above) and pLOW-*ftsZ-*
497 *mYFP* were digested with SalI and BamHI and subsequently ligated, resulting in pLOW-*smdA-*
498 *mYFP*.
499
500 **CRISPRi constructs**
501 *Construction of pCG248-sgRNA(smdA).* For gene knockdowns, the CRISPR interference
502 (CRISPRi) system developed by Stamsås et al. (69) was used. In this system, *dcas9* is placed
503 downstream of an IPTG-inducible promoter in the plasmid pLOW-*dcas9*. A second plasmid is
504 carrying the single guide RNA (pCG248-sgRNA(*x*), where *x* represents the targeted gene),
505 which constitutively expresses the sgRNA, including the 20 nt base-pairing region specific for
506 the gene to be knocked down. The pLOW-*dcas9* plasmid contains an erythromycin resistance
507 gene, and the pCG248-sgRNA(*x*) plasmid a chloramphenicol resistance gene. The gene-
508 specific 20 nt sequences were replaced in the pCG248-sgRNA(*x*) plasmids using an inverse
509 PCR approach as described earlier (69) using primers mk299 and mk323.
510
511 *Construction of pLOW-dCas9_aad9.* In order to make the CRISPRi system compatible with
512 the MRSA strain COL (which is intrinsically erythromycin resistant), the erythromycin
513 resistance gene *ermC* in pLOW-*dcas9* was replaced with *aad9*, encoding a spectinomycin
514 resistance cassette. The primers im183 and im184 were used to amplify the entire pLOW-*dcas9*

515 plasmid, except the *ermC* gene. The *aad9* gene was amplified with primers im185 and im186
516 using pCN55 (70) as template, where im185 contained the sequence of im183 as overhang, and
517 im186 the sequence of im184 as overhang. Thus, the two fragments had overlapping sequences
518 and were fused using NEBuilder® HiFi DNA Assembly (NEB). The construct was transformed
519 to *E. coli* IM08B, and the plasmid verified by PCR and sequencing. For CRISPRi in *S. aureus*
520 COL, the pLOW-*dcas9_aad9* plasmid was used along with pCG248-sgRNA(*x*).
521

522 **Construction of plasmids used for overexpression studies**

523 <u>*Construction of pLOW-smdA and mutated versions.*</u> *smdA* was amplified from *S. aureus*
524 genomic DNA using primers im77_SA1908_F_SalI_RBS and mk517_1908_R_NotI. The
525 fragment was digested with SalI and NotI and ligated into the corresponding sites of plasmid
526 pLOW-*dcas9* (69) to produce the plasmid pLOW-*smdA*, with IPTG-inducible overexpression
527 of *smdA*. pLOW-*smdAΔTMH* was constructed in a similar manner, except that primer
528 mk518_1908_F_RBS_SalI was used instead of im77 to remove the 29 N-terminal amino acids
529 of SmdA, predicted to encode the TMH and extracellular part. Site-directed mutagenesis in the
530 two plasmids was performed by a two-step overlap extension PCR approach, where the
531 mutations were introduced in the primers. The primers mk519 and mk520 were used for
532 introducing mutation H145A (mut1), mut2 (R150A, R151A) was made with primers mk521
533 and mk522, and mut3 (F280A, H281A) with primers mk529 and mk530.
534

535 **Phase contrast- and fluorescence microscopy analysis**

536 For induction of plasmid-encoded fluorescent fusions, exponentially growing cultures were
537 diluted to OD_{600} 0.05 in medium with 50 µM IPTG an incubated for 2 hours prior to
538 microscopy. For CRISPRi-knockdown and overexpression experiments, cultures of OD_{600} =
539 0.4 were diluted 250-fold in medium with 300 µM IPTG and grown until OD_{600} was

540 approximately 0.4. For labelling of cell wall, BODIPY^{TM} FL vancomycin (VanFL) (Invitrogen)
541 was added. To label newly synthesized peptidoglycan, HADA (van Nieuwenhze group, Indiana
542 University) was added actively growing cultures (OD_{600} approximately 0.4) at a final
543 concentration of 250 μM. The cells were incubated with HADA at 37°C for 90 sec and then
544 put on ice. The cultures were pelleted by centrifugation at 10 000 × *g* at 4°C for 1 min, washed
545 with cold 1 × PBS, pH 7.4 and finally resuspended in 25 μl PBS. Cells were subsequently
546 added to agarose pads and microscopy was performed on a Zeiss AxioObserver with ZEN Blue
547 software. An ORCAFlash4.0 V2 Digital complementary metal-oxide semiconductor (CMOS)
548 camera (Hamamatsu Photonics) was used to capture images through a 100 × PC objective.
549 HPX 120 Illuminator (Zeiss) was used as a light source for fluorescence microscopy.
550 All microscopy analyses were repeated at least two times. Images were processed and
551 prepared for publication using Fiji (71). For analysis of cell roundness, cell area and fluorescent
552 labelling patterns, MicrobeJ (72) was used to determine cell outlines. Outlines were corrected
553 manually, when necessary. Cell area and roundness as a measure of morphology were
554 calculated and plotted using MicrobeJ. After cell outline detection, categorization of cells into
555 normal or abnormal labelling patterns were done manually using images from independent
556 experiments. The septum/periphery fluorescence signal ratio was measured as described before
557 (73) in cells with full septal signal of SmdA-GFP. A fluoresce ratio between 2.5 and 3.5 is
558 typical for septum-enriched proteins (11).
559
560 **Structured illumination microscopy (SIM) and stimulated emission depletion (STED)**
561 **microscopy**
562 Super-resolution SIM imaging was performed using a Zeiss ELYRA PS.1 microscope
563 equipped with a 100 × 1.46 NA alpha plan apochromat oil immersion objective and a pco.edge
564 sCMOS camera. Fluorescence images were acquired sequentially using 200–300 ms exposure

565 times per image, for a total of 15 images per SIM reconstruction. All imaging was performed
566 at room temperature (~23°C). Raw data were reconstructed using the SIM algorithms in ZEN
567 2011 SP7 software (black edition, Carl Zeiss). Brightfield images were captured using
568 widefield imaging mode. Images had a final pixel size of 25 nm.

569 Gated STED (gSTED) images were acquired on a Leica TCS SP8 STED 3× system,
570 using an HC PL Apo 100 × oil immersion objective with NA 1.40. Fluorophores were excited
571 using a white excitation laser operated at 509 nm for mYFP and 563 nm for mKate2. A STED
572 depletion laser line was operated at 592 nm and 775 nm for mYFP and mKate2, respectively,
573 using a detection time-delay of 0.8–1.6 ns for both fluorophores. The total depletion laser
574 intensity was in the order of 20–40 MW cm^{-2} for all STED imaging. The final pixel size was
575 13 nm and scanning speed was 400 Hz. The pinhole size was set to 0.9 AU.

576 Images were processed and analyzed using Fiji (71). Line scans were analyzed using
577 the Plot Profile function in Fiji, using a line width of 1.5. Fluorescence intensities were
578 normalized to the highest value for each channel.

579

580 **Scanning- and transmission electron microscopy analysis**

581 Overnight cultures were diluted to approximately OD_{600} = 0.1. When OD_{600} reached 0.4, the
582 cultures were diluted 1:250. Antibiotic and IPTG were added when appropriate. The cultures
583 (10 ml) were grown to OD_{600} = 0.3 and 1 volume of fixation solution, containing 5 % (w/v)
584 glutaraldehyde and 4 % (w/v) paraformaldehyde in 1×PBS, pH 7.4, was added. The tubes were
585 carefully inverted a few times and incubated for one hour at room temperature before being
586 placed at 4°C overnight. The following day, the cultures were centrifugated at 5000 × *g*, and
587 the pellets washed three times with PBS. Further preparations of samples to be analyzed with
588 TEM were performed as described before (69).

589 Samples for SEM were, after washing with PBS, dehydrated with EtOH, essentially in
590 the same manner as for sample preparations for TEM (69). The samples were subjected to
591 critical point drying by exchanging the EtOH with CO_2. Then, the samples were coated with a
592 conductive layer of Au-Pd before being analyzed in a ZEISS EVO50 EP Scanning electron
593 microscope. Images were analyzed and prepared using Fiji (71).
594
595 **Growth assays**
596 For examining growth on solid media, overnight cultures were diluted 1:250 in BHI containing
597 300 µM IPTG, unless otherwise specified. When reaching exponential phase, OD_{600} were
598 adjusted to 0.3 for all samples. A 10-fold dilution series were made for all strains, and 2 µl of
599 each dilution were spotted on BHI agar containing proper antibiotics and 300 µM IPTG. The
600 plates were incubated at 37°C for approximately 16 h, and pictures of the plates were captured
601 in a Gel Doc™ XR + Imager (Bio-Rad).
602 For measurement of growth in liquid cultures, cells were at OD_{600} 0.4, were diluted
603 1:250 in medium containing 300 µM IPTG. Every hours for five hours, OD_{600} was measured
604 spectrophotometrically using Genesys 30 (Thermo Scientific) and dilutions of the cultures were
605 plated for CFU-counting.
606
607 **Minimum inhibitory concentration (MIC) assays**
608 The experiments were set up in 96-well microtiter plates with a total volume of 300 µl. A two-
609 fold dilution series of the antibiotics were prepared in BHI containing selective antibiotics and
610 IPTG when appropriate. The overnight cultures were diluted 1:1000 in BHI containing 300
611 µg/ml IPTG for induction. The cells were grown at 37°C, and the plate was shaken for 5 sec
612 before measurements of OD_{600} were taken every 10th min throughout the experiment, using

613 either a Synergy™ H1 Hybrid Multi-Mode Reader (BioTek Instruments) or a Hidex Sense
614 (Hidex Oy). The experiments were repeated at least two times with the same results.
615
616 **RNA isolation and RT-PCR**
617 To verify that *smdA* expression was knocked down by CRISPRi, RNA was isolated from
618 exponentially growing cultures of IM284 (SH1000, CRISPRi(control)), IM165 (SH000
619 CRISPRi(empty)) and IM269 (SH1000 CRISPRi(*smdA*)). Isolation of total RNA and cDNA
620 synthesis were performed as previously described (69). A PCR reaction (30 cycles) was run
621 with Phusion® High-Fidelity DNA polymerase (NEB). The primer pairs im126/im127 and
622 im137/im138 were used to target the reference gene *pta* (74) and *smdA*, respectively.
623
624 **Detection of lipoteichoic acid (LTA) by Western blotting**
625 Detection of LTA was performed by western blotting, and sample preparations were done
626 according to descriptions found in Hesser et al (26). The samples were separated on a 4-20 %
627 gradient Mini Protean TGX acrylamide gel (BioRad), and subsequently transferred to a
628 polyvinylidene difluoride (PVDF) membrane by semi-dry electroblotting. The membrane was
629 blocked for 1 h in 5 % (w/v) skim milk in PBST and placed overnight at 4°C. Next, the
630 membrane was incubated for 1 h with α-LTA (Hycult) 1:4000 in PBST, washed three times
631 (10 minutes each) with PBST before incubation for 1 h with α-Mouse IgG HRP Conjugate
632 (Promega) secondary antibody (1:10 000 in PBST). The membrane was again washed three
633 times and LTA bands were visualized by using SuperSignal™ West Pico PLUS
634 Chemiluminescent substrate (Thermo Fisher Scientific) in an Azure Imager c400 (Azure
635 Biosystems).
636 Same procedure as in (44) was carried out for possible detection of LTA released to the
637 medium. The supernatants, after harvesting cells during sample preparations, were kept.

638 Supernatant samples were centrifugated for 16 000 × *g* for 10 min, and 75 µl was mixed with
639 25 µl 4 × SDS-PAGE sample buffer. These samples were boiled for 30 min and applied on the
640 4-20 % Mini Protean TGX acrylamide gel. Thereafter, the same immunodetection procedure
641 as described above was followed.
642
643 **Fourier-transform infrared spectroscopy (FTIR) analysis**
644 Cultures of the strains IM313 (HG001, CRISPRi(control)), IM312 (HG001, CRISPRi(*smdA*))
645 and IM357 (HG001, CRISPRi(*tarO*)) were initially pre-grown to exponential phase, back
646 diluted to OD_{600} = 0.05 and induced with 300 µM IPTG. The bacterial cells (1 ml) were
647 harvested at OD_{600} = 0.4 by centrifugation at 5000 × *g*, 4°C, for 3 min. The pelleted cells were
648 kept at -20°C prior to further processing. Pellets were resuspended in 40 µl 0.1 % (w/v) NaCl,
649 and 10 µl of the suspensions were added to an IR-light-transparent silicon 384-well microplate
650 (Bruker Optic, Germany), with three technical replicates for each sample. The plates were left
651 to dry at room temperature for approximately 2 h. FTIR spectra were recorded in transmission
652 mode using a high-throughput screening extension (HTS-XT) unit coupled to a Vertex 70 FTIR
653 spectrometer (Bruker Optik GmbH, Leipzig, Germany). Spectra were recorded in the region
654 4000-500 cm^{-1}, with a spectral resolution of 6 cm^{-1}, a digital spacing of 1.928 cm^{-1}, and an
655 aperture of 5 mm. For each spectrum, 64 scans were averaged. The OPUS software (Bruker
656 Optik GmbH, Leipzig,Germany) was used for data acquisition and instrument control. The
657 obtained spectra were processed by taking second derivatives and extended multiplicative
658 signal correction (EMSC) preprocessing in Unscrambler X version 11 (CAMO Analytics,
659 Oslo, Norway). Results presented are averaged spectra from 3 biological replicates (each with
660 3 technical replicates) for the region with wavelengths between 1200 cm^{-1} and 800 cm^{-1}.
661

662 **GFP-trap and liquid chromatography with tandem mass spectrometry (LC-MS/MS)**

663 Cultures (*S. aureus* SH1000 wild-type, IM308 SH1000 *smdA-m(sf)gfp*, IM104 SH1000
664 pLOW-*smdA-m(sf)gfp* and IM164 SH1000 pLOW-*smdA-flag*) were pre-grown to exponential
665 phase, back diluted to OD_{600} = 0.05 and induced if necessary. When reaching OD_{600} at 0.4, 80
666 ml of each culture were harvested by centrifugation at 4000 × *g*, 4°C for 3 min. Supernatants
667 were decanted and pellets resuspended in cold TBS prior to transfer to 1.5 ml microcentrifuge
668 tubes. Centrifugation was repeated for 1 min, and pelleted cells were stored at -80°C prior to
669 further use.

670 For GFP-trap, cells were resuspended in 1 ml cold buffer containing 10 mM Tris pH
671 7.5, 150 mM NaCl, 1 mM PMSF, 6 µg/ml RNase and 6 µg/ml DNase. Suspensions were
672 transferred to 2 ml lysing matrix B tubes (MP Biomedicals) containing 0.8 g ≤ 106 µm glass
673 beads (Sigma-Aldrich) and subjected for mechanical lysis by agitation in a FastPrep-24™ (MP
674 Biomedicals) for 3 × 30 sec at 6.5 m/s, with 1 min pause on ice between the runs. Tubes were
675 centrifugated at 5000 × *g*, 4°C for 10 min, and supernatants transferred to new tubes.
676 Concentrations were determined measuring Abs280 using NanoDrop™ 2000 (Thermo Fisher
677 Scientific), where a small amount of the samples were added a final concentration of 1 % (w/v)
678 SDS prior to measurements. GFP-Trap beads (25 µl per sample) (Chromotek) were washed
679 three times with 500 µl ice cold Dilution/Wash buffer (10 mM Tris pH 7.5, 150 mM NaCl, 0.5
680 mM EDTA) and centrifugated at 2500 × *g*, 4°C for 5 min. Lysates were diluted in
681 Dilution/Wash buffer to a final concentration of 1 mg in a total volume of 500 µl, before being
682 transferred to GFP-Trap beads. Samples were placed in a Bio RS-24 Multi rotor (Biosan) at
683 4°C for 1 h. Then, samples were centrifugated at 2500 × *g*, 4°C for 5 min, supernatant removed,
684 and beads washed three times with Dilution/Wash buffer. During last washing step, solutions
685 were transferred to new tubes, and after centrifugation and removal of supernatant, beads were
686 resuspended in 50 µl 5 % (w/v) SDS, 50 mM Tris pH 7.6. Tubes were incubated at 95°C for 5

687 min, and centrifugated at maximum speed for 30 sec. After standing at the bench a few minutes,
688 30-50 µl were transferred into new tubes. Samples were kept at -20°C and heated for 2 min at
689 95°C prior to the sample preparation method Suspension trapping (STrap), conducted as
690 described by A. Zougman et al. (75).

691 The peptide samples were analyzed by coupling a nano UPLC (nanoElute, Bruker) to a
692 trapped ion mobility spectrometry/quadrupole time of flight mass spectrometer (timsTOF Pro,
693 Bruker). The peptides were separated by an Aurora Series 1.6 µm C18 reverse-phase 25 cm ×
694 75 µm analytical column with nanoZero and CaptiveSpray Insert (IonOpticks, Australia). The
695 flow rate was set to 400 nl/min and the peptides were separated using a gradient from 2 % to
696 95 % acetonitrile solution (in 0.1 % (v/v) formic acid) over 120 minutes. The timsTOF Pro was
697 ran in positive ion data dependent acquisition PASEF mode, with a mass range at 100-1700
698 m/z. The acquired spectra were analyzed against a *S. aureus* NCTC8325 proteome database.
699

700 **Bacterial two-hybrid (BACTH) assays**

701 Plasmid construction, and procedure for the BACTH assays, were conducted in a same manner
702 as previously described (69), and primers used are listed in Table S3. Briefly, gene fusions of
703 selected genes, to the T18 or T25 domains of adenylate cyclase form *Bordetella pertussis,* were
704 made by restriction cutting and ligation in the plasmid vectors pKT25, pKNT25, pUT18 or
705 pUT18C (Euromedex). *E. coli* XL1-Blue cells were used for transformation, and plasmids
706 verified by sequencing before BACTH assays (76) were set up according to the manufacturer
707 (Euromedex). Co-transformation of plasmids containing fusion-genes of opposite domains,
708 that is T25 in one plasmid and T18 in the other, were done in *E. coli* BTH101 with 50 µg/ml
709 kanamycin and 100 µg/ml ampicillin as selection markers. Five random colonies were picked,
710 grown in liquid LB to visible growth, and spotted on LA plates containing 40 µg/ml X-gal and
711 0.5 mM IPTG, in addition to the selection markers. Plates were incubated dark at 30°C for 20-

712 48 h before being inspected, and blue colonies are an indication of positive interaction between
713 tested genes. Presented results are representative for at least six independent replicates.
714

715 ## Acknowledgements

716 We would like to acknowledge the NMBU Imaging Center for help with electron microscopy,
717 Maria Victoria Heggenhougen and Marita Torrissen Mårli (both NMBU) for access to
718 unpublished strains and Henriette Olsen (NMBU) for help with FTIR. Mass spectrometry-
719 based proteomic analyses were performed by The MS and Proteomics Core Facility,
720 Norwegian University of Life Sciences (NMBU). This facility is a member of the National
721 Network of Advanced Proteomics Infrastructure (NAPI), which is funded by the Research
722 Council of Norway INFRASTRUKTUR-program (project number: 295910). We acknowledge
723 the van Nieuwenhze group, Indiana University, for providing HADA. The work is supported
724 by grants from the Research Council of Norway (project number 250976) and JPI-AMR
725 (project number 296906). Work in the Structural Cell Biology Unit (OIST) is supported by
726 OIST core subsidy. Ine S. Myrbråten acknowledge support from "Pasteurlegatet".

727

728 ## References

729 1. Sass P, Brötz-Oesterhelt H. 2013. Bacterial cell division as a target for new antibiotics.
730 Curr Opin Microbiol 16:522-530.
731 2. Pinho MG, Kjos M, Veening J-W. 2013. How to get (a) round: mechanisms controlling
732 growth and division of coccoid bacteria. Nat Rev Microbiol 11:601-614.
733 3. Errington J, Daniel RA, Scheffers D-J. 2003. Cytokinesis in bacteria. Microbiol Mol
734 Biol Rev 67:52-65.
735 4. Saraiva BM, Sorg M, Pereira AR, Ferreira MJ, Caulat LC, Reichmann NT, Pinho MG.
736 2020. Reassessment of the distinctive geometry of *Staphylococcus aureus* cell division.
737 Nat Comm 11:1-7.
738 5. Veiga H, Jorge AM, Pinho MG. 2011. Absence of nucleoid occlusion effector Noc
739 impairs formation of orthogonal FtsZ rings during *Staphylococcus aureus* cell division.
740 Mol Microbiol 80:1366-1380.
741 6. Gallay C, Sanselicio S, Anderson ME, Soh YM, Liu X, Stamsås GA, Pelliciari S, van
742 Raaphorst R, Dénéréaz J, Kjos M, Murray H, Gruber S, Grossman AD, Veening JW.
743 2021. CcrZ is a pneumococcal spatiotemporal cell cycle regulator that interacts with
744 FtsZ and controls DNA replication by modulating the activity of DnaA. Nat Microbiol
745 6:1175-1187.
746 7. Barreteau H, Kovač A, Boniface A, Sova M, Gobec S, Blanot D. 2008. Cytoplasmic
747 steps of peptidoglycan biosynthesis. FEMS Microbiol Rev 32:168-207.
748 8. Bouhss A, Trunkfield AE, Bugg TD, Mengin-Lecreulx D. 2007. The biosynthesis of
749 peptidoglycan lipid-linked intermediates. FEMS Microbiol Rev 32:208-233.
750 9. Rohrer S, Berger-Bächi B. 2003. FemABX peptidyl transferases: a link between
751 branched-chain cell wall peptide formation and β-lactam resistance in gram-positive
752 cocci. Antimicrob Agents Chemother 47:837-846.
753 10. Sham L-T, Butler EK, Lebar MD, Kahne D, Bernhardt TG, Ruiz N. 2014. Bacterial cell
754 wall. MurJ is the flippase of lipid-linked precursors for peptidoglycan biogenesis.
755 Science 345:220-222.
756 11. Monteiro JM, Pereira AR, Reichmann NT, Saraiva BM, Fernandes PB, Veiga H,
757 Tavares AC, Santos M, Ferreira MT, Macario V, VanNieuwenhze MS, Filipe SR, Pinho
758 MG. 2018. Peptidoglycan synthesis drives an FtsZ-treadmilling-independent step of
759 cytokinesis. Nature 554:528-532.

760 12. Reichmann NT, Tavares AC, Saraiva BM, Jousselin A, Reed P, Pereira AR, Monteiro
761 JM, VanNieuwenhze MS, Fernandes F, Pinho MG. 2019. SEDS-bPBP pairs direct
762 lateral and septal peptidoglycan synthesis in *Staphylococcus aureus*. Nat Microbiol
763 4:1368-1377.
764 13. Meeske AJ, Riley EP, Robins WP, Uehara T, Mekalanos JJ, Kahne D, Walker S, Kruse
765 AC, Bernhardt TG, Rudner DZ. 2016. SEDS proteins are a widespread family of
766 bacterial cell wall polymerases. Nature 537:634-638.
767 14. Wyke AW, Ward JB, Hayes MV, Curtis NA. 1981. A role *in vivo* for penicillin-binding
768 protein-4 of *Staphylococcus aureus*. Eur J Biochem 119:389-393.
769 15. Atilano ML, Pereira PM, Yates J, Reed P, Veiga H, Pinho MG, Filipe SR. 2010.
770 Teichoic acids are temporal and spatial regulators of peptidoglycan cross-linking in
771 *Staphylococcus aureus*. Proc Natl Acad Sci U S A 107:18991-18996.
772 16. Pinho MG, Errington J. 2005. Recruitment of penicillin-binding protein PBP2 to the
773 division site of *Staphylococcus aureus* is dependent on its transpeptidation substrates.
774 Mol Microbiol 55:799-807.
775 17. Hartman BJ, Tomasz A. 1984. Low-affinity penicillin-binding protein associated with
776 beta-lactam resistance in *Staphylococcus aureus*. J Bacteriol 158:513-516.
777 18. Ubukata K, Yamashita N, Konno M. 1985. Occurrence of a beta-lactam-inducible
778 penicillin-binding protein in methicillin-resistant staphylococci. Antimicrob Agents
779 Chemother 27:851-857.
780 19. Oshida T, Sugai M, Komatsuzawa H, Hong Y-M, Suginaka H, Tomasz A. 1995. A
781 *Staphylococcus aureus* autolysin that has an N-acetylmuramoyl-L-alanine amidase
782 domain and an endo-beta-N-acetylglucosaminidase domain: cloning, sequence
783 analysis, and characterization. Proc Natl Acad Sci U S A 92:285-289.
784 20. Nega M, Tribelli PM, Hipp K, Stahl M, Götz F. 2020. New insights in the coordinated
785 amidase and glucosaminidase activity of the major autolysin (Atl) in *Staphylococcus*
786 *aureus*. Commun Biol 3:1-10.
787 21. Thalsø-Madsen I, Torrubia FR, Xu L, Petersen A, Jensen C, Frees D. 2019. The Sle1
788 cell wall amidase is essential for β-lactam resistance in community-acquired
789 methicillin-resistant *Staphylococcus aureus* USA300. Antimicrob Agents Chemother
790 64:e01931-19.
791 22. Dubrac S, Boneca IG, Poupel O, Msadek T. 2007. New insights into the WalK/WalR
792 (YycG/YycF) essential signal transduction pathway reveal a major role in controlling

793 cell wall metabolism and biofilm formation in *Staphylococcus aureus*. J Bacteriol
794 189:8257-69.
795 23. Zhou X, Halladin DK, Rojas ER, Koslover EF, Lee TK, Huang KC, Theriot JA. 2015.
796 Mechanical crack propagation drives millisecond daughter cell separation in
797 *Staphylococcus aureus*. Science 348:574-578.
798 24. Monteiro JM, Fernandes PB, Vaz F, Pereira AR, Tavares AC, Ferreira MT, Pereira PM,
799 Veiga H, Kuru E, VanNieuwenhze MS. 2015. Cell shape dynamics during the
800 staphylococcal cell cycle. Nat Comm 6:1-12.
801 25. Brown S, Santa Maria Jr JP, Walker S. 2013. Wall teichoic acids of Gram-positive
802 bacteria. Ann Rev Microbiol 67:313-336.
803 26. Hesser AR, Matano LM, Vickery CR, Wood BM, Santiago AG, Morris HG, Do T,
804 Losick R, Walker S. 2020. The length of lipoteichoic acid polymers controls
805 *Staphylococcus aureus* cell size and envelope integrity. J Bacteriol 202:e00149-20.
806 27. Silber N, Pan S, Schäkermann S, Mayer C, Brötz-Oesterhelt H, Sass P. 2020. Cell
807 division protein FtsZ is unfolded for N-terminal degradation by antibiotic-activated
808 ClpP. mBio 11:e01006-20.
809 28. Feng J, Michalik S, Varming AN, Andersen JH, Albrecht D, Jelsbak L, Krieger S,
810 Ohlsen K, Hecker M, Gerth U, Ingmer H, Frees D. 2013. Trapping and proteomic
811 identification of cellular substrates of the ClpP protease in *Staphylococcus aureus*. J
812 Proteome Res 12:547-58.
813 29. Jensen C, Bæk KT, Gallay C, Thalsø-Madsen I, Xu L, Jousselin A, Torrubia FR,
814 Paulander W, Pereira AR, Veening J-W. 2019. The ClpX chaperone controls autolytic
815 splitting of *Staphylococcus aureus* daughter cells, but is bypassed by β-lactam
816 antibiotics or inhibitors of WTA biosynthesis. PLoS Pathog 15:e1008044.
817 30. Chaudhuri RR, Allen AG, Owen PJ, Shalom G, Stone K, Harrison M, Burgis TA,
818 Lockyer M, Garcia-Lara J, Foster SJ, Pleasance SJ, Peters SE, Makell DJ, Charles IG.
819 2009. Comprehensive identification of essential *Staphylococcus aureus* genes using
820 Transposon-Mediated Differential Hybridisation (TMDH). BMC Genomics 10:291.
821 31. Santiago M, Matano LM, Moussa SH, Gilmore MS, Walker S, Meredith TC. 2015. A
822 new platform for ultra-high density *Staphylococcus aureus* transposon libraries. BMC
823 Genomics 16:1-18.
824 32. Valentino MD, Foulston L, Sadaka A, Kos VN, Villet RA, Santa Maria J, Lazinski DW,
825 Camilli A, Walker S, Hooper DC. 2014. Genes contributing to *Staphylococcus aureus*
826 fitness in abscess-and infection-related ecologies. mBio 5:e01729-14.

827 33. Grynberg M, Godzik A. 2004. NERD: a DNA processing-related domain present in the
828 anthrax virulence plasmid, pXO1. Trends Biochem Sci 29:106-110.
829 34. Arnaud M, Chastanet A, Débarbouillé M. 2004. New vector for efficient allelic
830 replacement in naturally nontransformable, low-GC-content, Gram-positive bacteria.
831 Appl Environ Microbiol 70:6887-6891.
832 35. Liew AT, Theis T, Jensen SO, Garcia-Lara J, Foster SJ, Firth N, Lewis PJ, Harry EJ.
833 2011. A simple plasmid-based system that allows rapid generation of tightly controlled
834 gene expression in *Staphylococcus aureus*. Microbiology 157:666-676.
835 36. Reynolds PE. 1989. Structure, biochemistry and mechanism of action of glycopeptide
836 antibiotics. Eur J Clin Microbiol Infect Dis 8:943-950.
837 37. Campbell J, Singh AK, Santa Maria Jr JP, Kim Y, Brown S, Swoboda JG, Mylonakis
838 E, Wilkinson BJ, Walker S. 2011. Synthetic lethal compound combinations reveal a
839 fundamental connection between wall teichoic acid and peptidoglycan biosyntheses in
840 *Staphylococcus aureus*. ACS Chem Biol 6:106-116.
841 38. Campbell J, Singh AK, Swoboda JG, Gilmore MS, Wilkinson BJ, Walker S. 2012. An
842 antibiotic that inhibits a late step in wall teichoic acid biosynthesis induces the cell wall
843 stress stimulon in *Staphylococcus aureus*. Antimicrob Agents Chemother 56:1810-20.
844 39. Vickery CR, Wood BM, Morris HG, Losick R, Walker S. 2018. Reconstitution of
845 *Staphylococcus aureus* lipoteichoic acid synthase activity identifies Congo red as a
846 selective inhibitor. J Am Chem Soc 140:876-879.
847 40. Price NP, Tsvetanova B. 2007. Biosynthesis of the tunicamycins: a review. J Antibiot
848 60:485-491.
849 41. Swoboda JG, Campbell J, Meredith TC, Walker S. 2010. Wall teichoic acid function,
850 biosynthesis, and inhibition. Chembiochem 11:35-45.
851 42. Santa Maria JP, Jr., Sadaka A, Moussa SH, Brown S, Zhang YJ, Rubin EJ, Gilmore
852 MS, Walker S. 2014. Compound-gene interaction mapping reveals distinct roles for
853 *Staphylococcus aureus* teichoic acids. Proc Natl Acad Sci U S A 111:12510-12515.
854 43. Oku Y, Kurokawa K, Matsuo M, Yamada S, Lee B-L, Sekimizu K. 2009. Pleiotropic
855 roles of polyglycerolphosphate synthase of lipoteichoic acid in growth of
856 *Staphylococcus aureus* cells. J Bacteriol 191:141-151.
857 44. Mikkelsen K, Sirisarn W, Alharbi O, Alharbi M, Liu H, Nøhr-Meldgaard K, Mayer K,
858 Vestergaard M, Gallagher LA, Derrick JP. 2021. The novel membrane-associated
859 auxiliary factors AuxA and AuxB modulate β-lactam resistance in MRSA by stabilizing
860 lipoteichoic acids. Int J Antimicrob Agents 57:106283.

861 45. Suzuki T, Campbell J, Kim Y, Swoboda JG, Mylonakis E, Walker S, Gilmore MS.
862 2012. Wall teichoic acid protects *Staphylococcus aureus* from inhibition by Congo red
863 and other dyes. J Antimicrob Chemother 67:2143-2151.
864 46. Chan YG-Y, Kim HK, Schneewind O, Missiakas D. 2014. The capsular polysaccharide
865 of *Staphylococcus aureus* is attached to peptidoglycan by the LytR-CpsA-Psr (LCP)
866 family of enzymes. J Biol Chem 289:15680-15690.
867 47. Grunert T, Jovanovic D, Sirisarn W, Johler S, Weidenmaier C, Ehling-Schulz M, Xia
868 G. 2018. Analysis of *Staphylococcus aureus* wall teichoic acid glycoepitopes by
869 Fourier Transform Infrared Spectroscopy provides novel insights into the
870 staphylococcal glycocode. Sci Rep 8:1-9.
871 48. Radkov AD, Hsu Y-P, Booher G, VanNieuwenhze MS. 2018. Imaging bacterial cell
872 wall biosynthesis. Annu Rev Biochem 87:991-1014.
873 49. Biswas R, Voggu L, Simon UK, Hentschel P, Thumm G, Götz F. 2006. Activity of the
874 major staphylococcal autolysin Atl. FEMS Microbiol Letters 259:260-268.
875 50. Jorge AM, Hoiczyk E, Gomes JP, Pinho MG. 2011. EzrA contributes to the regulation
876 of cell size in *Staphylococcus aureus*. PLoS One 6:e27542.
877 51. Lund VA, Wacnik K, Turner RD, Cotterell BE, Walther CG, Fenn SJ, Grein F,
878 Wollman AJ, Leake MC, Olivier N, Cadby A, Mesnage S, Jones S, Foster SJ. 2018.
879 Molecular coordination of *Staphylococcus aureus* cell division. eLife 7:e32057.
880 52. Jumper J, Evans R, Pritzel A, Green T, Figurnov M, Ronneberger O, Tunyasuvunakool
881 K, Bates R, Žídek A, Potapenko A, Bridgland A, Meyer C, Kohl SAA, Ballard AJ,
882 Cowie A, Romera-Paredes B, Nikolov S, Jain R, Adler J, Back T, Petersen S, Reiman
883 D, Clancy E, Zielinski M, Steinegger M, Pacholska M, Berghammer T, Bodenstein S,
884 Silver D, Vinyals O, Senior AW, Kavukcuoglu K, Kohli P, Hassabis D. 2021. Highly
885 accurate protein structure prediction with AlphaFold. Nature 596:583-589.
886 53. Roemer T, Schneider T, Pinho MG. 2013. Auxiliary factors: a chink in the armor of
887 MRSA resistance to β-lactam antibiotics. Curr Opin Microbiol 16:538-548.
888 54. Tan CM, Therien AG, Lu J, Lee SH, Caron A, Gill CJ, Lebeau-Jacob C, Benton-
889 Perdomo L, Monteiro JM, Pereira PM, Elsen NL, Wu J, Deschamps K, Petcu M, Wong
890 S, Daigneault E, Kramer S, Liang L, Maxwell E, Claveau D, Vaillancourt J, Skorey K,
891 Tam J, Wang H, Meredith TC, Sillaots S, Wang-Jarantow L, Ramtohul Y, Langlois E,
892 Landry F, Reid JC, Parthasarathy G, Sharma S, Baryshnikova A, Lumb KJ, Pinho MG,
893 Soisson SM, Roemer T. 2012. Restoring methicillin-resistant *Staphylococcus aureus*
894 susceptibility to β-lactam antibiotics. Sci Transl Med 4:126ra35.

895 55. Lee SH, Jarantow LW, Wang H, Sillaots S, Cheng H, Meredith TC, Thompson J,
896 Roemer T. 2011. Antagonism of chemical genetic interaction networks resensitize
897 MRSA to β-lactam antibiotics. Chem Biol 18:1379-1389.
898 56. Brown S, Xia G, Luhachack LG, Campbell J, Meredith TC, Chen C, Winstel V, Gekeler
899 C, Irazoqui JE, Peschel A. 2012. Methicillin resistance in *Staphylococcus aureus*
900 requires glycosylated wall teichoic acids. Proc Natl Acad Sci U S A 109:18909-18914.
901 57. Quiblier C, Zinkernagel AS, Schuepbach RA, Berger-Bächi B, Senn MM. 2011.
902 Contribution of SecDF to *Staphylococcus aureus* resistance and expression of virulence
903 factors. BMC Microbiol 11:72.
904 58. Roch M, Lelong E, Panasenko OO, Sierra R, Renzoni A, Kelley WL. 2019.
905 Thermosensitive PBP2a requires extracellular folding factors PrsA and HtrA1 for
906 *Staphylococcus aureus* MRSA β-lactam resistance. Commun Biol 2:417.
907 59. Pereira AR, Hsin J, Król E, Tavares AC, Flores P, Hoiczyk E, Ng N, Dajkovic A, Brun
908 YV, VanNieuwenhze MS, Roemer T, Carballido-Lopez R, Scheffers DJ, Huang KC,
909 Pinho MG. 2016. FtsZ-dependent elongation of a coccoid bacterium. mBio 7:e00908-
910 16.
911 60. Steele VR, Bottomley AL, Garcia-Lara J, Kasturiarachchi J, Foster SJ. 2011. Multiple
912 essential roles for EzrA in cell division of *Staphylococcus aureus*. Mol Microbiol
913 80:542-55.
914 61. Steczkiewicz K, Muszewska A, Knizewski L, Rychlewski L, Ginalski K. 2012.
915 Sequence, structure and functional diversity of PD-(D/E)XK phosphodiesterase
916 superfamily. Nucleic Acids Res 40:7016-7045.
917 62. Kwon A, Scott S, Taujale R, Yeung W, Kochut KJ, Eyers PA, Kannan N. 2019. Tracing
918 the origin and evolution of pseudokinases across the tree of life. Sci Signal
919 12:eaav3810.
920 63. Herbert S, Ziebandt AK, Ohlsen K, Schafer T, Hecker M, Albrecht D, Novick R, Gotz
921 F. 2010. Repair of global regulators in *Staphylococcus aureus* 8325 and comparative
922 analysis with other clinical isolates. Infect Immun 78:2877-89.
923 64. Monk IR, Tree JJ, Howden BP, Stinear TP, Foster TJ. 2015. Complete bypass of
924 restriction systems for major *Staphylococcus aureus* lineages. mBio 6:e00308-15.
925 65. Löfblom J, Kronqvist N, Uhlén M, Ståhl S, Wernérus H. 2007. Optimization of
926 electroporation-mediated transformation: *Staphylococcus carnosus* as model organism.
927 J Appl Microbiol 102:736-747.

928 66. van Raaphorst R, Kjos M, Veening J-W. 2017. Chromosome segregation drives
929 division site selection in *Streptococcus pneumoniae*. Proc Natl Acad Sci U S A
930 114:E5959-E5968.
931 67. Kjos M, Veening JW. 2014. Tracking of chromosome dynamics in live *Streptococcus*
932 *pneumoniae* reveals that transcription promotes chromosome segregation. Mol
933 Microbiol 91:1088-105.
934 68. Brzoska AJ, Firth N. 2013. Two-plasmid vector system for independently controlled
935 expression of green and red fluorescent fusion proteins in *Staphylococcus aureus*. Appl
936 Environ Microbiol 79:3133-3136.
937 69. Stamsås GA, Myrbråten IS, Straume D, Salehian Z, Veening JW, Håvarstein LS, Kjos
938 M. 2018. CozEa and CozEb play overlapping and essential roles in controlling cell
939 division in *Staphylococcus aureus*. Mol Microbiol 109:615-632.
940 70. Charpentier E, Anton AI, Barry P, Alfonso B, Fang Y, Novick RP. 2004. Novel
941 cassette-based shuttle vector system for Gram-positive bacteria. Appl Environ
942 Microbiol 70:6076-6085.
943 71. Schindelin J, Arganda-Carreras I, Frise E, Kaynig V, Longair M, Pietzsch T, Preibisch
944 S, Rueden C, Saalfeld S, Schmid B. 2012. Fiji: an open-source platform for biological-
945 image analysis. Nat Methods 9:676-682.
946 72. Ducret A, Quardokus EM, Brun YV. 2016. MicrobeJ, a tool for high throughput
947 bacterial cell detection and quantitative analysis. Nat Microbiol 1:16077.
948 73. Pereira PM, Filipe SR, Tomasz A, Pinho MG. 2007. Fluorescence ratio imaging
949 microscopy shows decreased access of vancomycin to cell wall synthetic sites in
950 vancomycin-resistant Staphylococcus aureus. Antimicrob Agents Chemother 51:3627-
951 33.
952 74. Valihrach L, Demnerova K. 2012. Impact of normalization method on experimental
953 outcome using RT-qPCR in *Staphylococcus aureus*. J Microbiol Methods 90:214-216.
954 75. Zougman A, Selby PJ, Banks RE. 2014. Suspension trapping (STrap) sample
955 preparation method for bottom-up proteomics analysis. Proteomics 14:1006-1000.
956 76. Karimova G, Pidoux J, Ullmann A, Ladant D. 1998. A bacterial two-hybrid system
957 based on a reconstituted signal transduction pathway. Proc Natl Acad Sci U S A
958 95:5752-6.
959 77. Omasits U, Ahrens CH, Müller S, Wollscheid B. 2014. Protter: interactive protein
960 feature visualization and integration with experimental proteomic data. Bioinformatics
961 30:884-886.

962 78. Sievers F, Wilm A, Dineen D, Gibson TJ, Karplus K, Li W, Lopez R, McWilliam H,
963 Remmert M, Söding J, Thompson JD, Higgins DG. 2011. Fast, scalable generation of
964 high-quality protein multiple sequence alignments using Clustal Omega. Mol Syst Biol
965 7:539.

966

967 ## Figures and figure legends

968

969 **Fig. 1. Phenotypes resulting from depletion of SmdA.** (**A**) Predicted topology of SmdA using
970 Protter (77). SmdA is predicted to have one transmembrane (TM) helix with a short
971 extracellular N-terminus and a large intracellular domain. The sequence with predicted
972 similarity to the NERD domain is highlighted in yellow. (**B**) Growth on solid media of SmdA
973 knockdown strains (SmdA^{down}) in *S. aureus* SH1000 (IM269), NCTC8325-4 (IM311), HG001
974 (IM312) and COL (IM294). Strains carrying a non-targeting sgRNA were used as controls
975 (IM284, IM307, IM313 and IM295 for the respective strains). From non-induced overnight
976 cultures, 10-fold dilution series were made and spotted onto plates with 300 µM isopropyl-β-
977 D-thiogalactopyranoside (IPTG). (**C**) SmdA^{down} (IM269) and control strain (IM284) analyzed
978 by phase contrast- and fluorescence microscopy of cells stained with the cell wall label VanFL.
979 White arrows point at mis-shaped cells and cells with perturbed septum formation. Magnified
980 insets of representative cells are shown for the VanFL micrographs. Scale bars, 5 µm. (**D**)
981 Fraction of cells with multiple septa per cell for the SmdA^{down} strain IM269 (n = 225) and the
982 non-target control strain IM284 (n = 242) are plotted. The asterisks indicate significant
983 difference (Fisher's exact test, P<0.001). (**E**) Cell roundness, as determined using MicrobeJ,
984 was used as a measure of the morphology of the cells. Spherical cells will have values close to
985 1. Cell roundness measures for the control strain IM284 (n = 198) and the SmdA^{down} strain
986 IM269 (n = 191) are plotted. (**F**) Cell area (in µm^2) as determined using MicrobeJ of the control
987 strain IM284 (n = 198) and the SmdA^{down} strain IM269 (n = 191). In E and F, significant
988 differences between the distributions are indicted by asterisks (**, P < 0.001). P-values were
989 derived from a Mann-Whitney test.

990

991 **Fig. 2. SmdA^{down} in *S. aureus* SH1000 visualized by electron microscopy.** (**A**) Transmission
992 electron- and (**B**) scanning electron micrographs of SH1000 CRISPRi control strain (IM284)
993 and SH1000 SmdA^{down} (IM269). In (A), red arrows in the TEM micrographs point at lysed
994 cells. Representative examples of cells with parallel septa or multiple septa are shown. Green
995 arrows point to initiation of septum synthesis at multiple sites within the same cell. Different
996 magnifications are shown, indicated by the scale bars.

997

998 **Fig. 3. SmdA interacts with important cell division proteins and is necessary for proper**
999 **localization of EzrA and peptidoglycan synthesis.** (**A**) Protein-protein interactions tested
1000 with bacterial two-hybrid assays, where SmdA and SmdAΔTMH were tested against PBP1,
1001 PBP2, PBP3 and EzrA. The proteins were fused to the T18 or T25 domains as indicated. Blue
1002 bacterial spots and plus symbols indicate positive interactions and white spots and minus
1003 symbols indicate no interaction. **(B-D).** Micrographs of HADA labelled *S. aureus* NCTC8325-
1004 4 with depletion and overexpression of SmdA. Arrows point at cells with misplaced septum
1005 synthesis. Scale bars, 2 µm. **(B)** CRISPRi control strain, IM307 (**C**) SmdA^{down} strain, IM311
1006 and (**D**) SmdA overexpression strain, MK1866. (**E**) Frequency plot of cells with normal or
1007 abnormal HADA labelling pattern. Categorization of normal or abnormal labelling patterns are
1008 indicated. The number of cells analyzed were 259, 179 and 189 for B, C and D, respectively.
1009 The asterisks indicate significant difference from the control (Fisher's exact test, $P<0.001$). (**F**)
1010 Micrographs showing co-localization of EzrA-GFP and HADA incorporation in *S. aureus*
1011 SH1000 strains with (MK1952) or without (MK1953) knockdown of SmdA. Phase contrast-
1012 and fluorescence images of HADA labelling and GFP (EzrA-GFP) are shown. Scale bars, 2
1013 µm. Arrows point to cells with abnormal localization of both HADA and EzrA-GFP. (**G**)
1014 Frequencies of cells (from F) with normal or abnormal localization of HADA and EzrA-GFP
1015 are plotted. The number of cells analyzed were 285 (for MK1953) and 298 (for MK1952). The

1016 asterisks indicate significant difference form the respective controls (Fisher's exact test,
1017 P<0.001).
1018
1019 **Fig. 4**. Autolysis of *S. aureus* SH1000 depletion strains (control = IM284; $WalR^{down}$ = IM293;
1020 $SmdA^{down}$ = IM269) measured in presence of (**A**) 0.5 % Triton X-100 and (**B**) 100 ng/ml
1021 lysostaphin. Results presented as % of initial OD_{600}. Error bars represent standard error
1022 calculated from four technical replicates.
1023
1024 **Fig. 5. Subcellular localization analysis of SmdA.** (**A**) Micrographs of cells with induced
1025 expression of SmdA-m(sf)GFP from plasmid (top panel, IM104), native chromosomal
1026 expression of the SmdA-m(sf)GFP fusion protein (middle panel, IM308), and expression of
1027 SmdAΔTMH-m(sf)GFP from plasmid (bottom panel, IM373). Scale bars, 2 µm. (**B**) SIM
1028 images of fixed *S. aureus* SH1000 with plasmid-expressed SmdA-mYFP and FtsZ-mKate2
1029 (HC060). (**B-I**) Side-view of a cell showing that FtsZ localizes at septum before arrival of
1030 SmdA. As cell division progresses, (**B-II**) SmdA concentrates at sites where septum formation
1031 is initiated, and (**B-III**) displays a septal localization at the two septal membranes as FtsZ
1032 constricts and septum formation proceeds. (**B-IV**) Top-view of a cell showing the FtsZ-ring
1033 inside of the SmdA-ring. All scale bars, 0.5 µm. (**C**) STED images of fixed *S. aureus* SH1000
1034 with plasmid-expressed SmdA-mYFP and FtsZ-mKate2 (HC060), where line scans show
1035 fluorescence intensity of selected areas. (**C-I**) At an early stage of cell division, the rings of
1036 both SmdA and FtsZ have a similar diameter, but do not overlap in their distribution, and a
1037 heterogenous distribution with a patchy signal is observed. (**C-II**) Top-view of a cell as cell
1038 division progresses, with the FtsZ-ring laying inside of SmdA, approximately 100-150 nm
1039 apart from each other. (**C-III**) Side-view of a cell showing how FtsZ is located innermost, and
1040 how SmdA is located at the two septal membranes. Scale bars, 0.5 µm.

1041

1042 **Fig. 6. Membrane attachment and the NERD domain are important for SmdA function.**
1043 (**A**) HADA stained *S. aureus* NCTC8325-4 control cells not expressing any SmdA-variant
1044 (IM307) and cells overexpressing SmdAΔTMH (MK1911), SmdAΔTMH_mut1 (IM377),
1045 _mut2 (IM378) and _mut3 (IM379). Scale bars, 2 µm. (**B**) The frequency of cells from panel
1046 A with normal or abnormal HADA staining is plotted. The number of cells plotted were 259
1047 the control, 82 for SmdAΔTMH, 101 for _mut1, 113 for _mut2 and 122 for _mut3. The
1048 asterisks indicate significant difference form the control (Fisher's exact test, P<0.001). ns
1049 indicates that there is not significant difference from the control. (**C**) Structure of SmdA,
1050 predicted by AlphaFold (52), where (**C-I**) shows the structure colored by a "per-residue
1051 confidence score" (pLDDT) with dark blue pLDDT > 90, light blue 90 > pLDDT > 70, and
1052 yellow 70 > pLDDT > 50, (**C-II**) shows the structured domain magnified with the predicted
1053 NERD colored in green and residues that have been mutated in red. (**C-III**) A magnified inset
1054 of (II) with annotated residues. The positions of the mutated residues are indicated in red. (**D**)
1055 Growth assay on solid media of *S. aureus* NCTC8325-4 expressing SmdAΔTMH,
1056 SmdAΔTMH_mut1, _mut2 and _mut3.

1057

1058 # Figures and figure legends

1059

1060 **Table 1. Minimum inhibitory concentration (MIC, in µg/ml) of different antimicrobials**
1061 **when SmdA was depleted in *S. aureus* SH1000 and COL.**

Antibiotics	***S. aureus* SH1000 (MSSA)**			***S. aureus* COL (MRSA)**		
	SmdA^{down}	Control	Fold change	SmdA^{down}	Control	Fold change
Oxacillin	0.12	0.24	2	64-128	256	2-4
Cefotaxime	2	2	1	50	400	8
Cefoxitin	1	2	2	47-94	188	2-4
Imipenem	0.016	0.016	1	150	>300	>2
Vancomycin	2.5	2.5	1	2.5	2.5	1
Tetracycline	0.05	0.1-0.2	2-4	≥64	≥64	1
Ciprofloxacin	0.32	0.32	1	0.32	0.32	1
Tunicamycin	0.094	6	64	24	>96	>4
Targocil	1	1	1	1	1	1
Congo Red	256	>1024	>4	512-1024	>1024	≥2

1062

1063

1064 ## Legends to supplementary material

1065

1066 **Fig. S1. Multiple sequence alignment of SmdA from different staphylococcal species.**
1067 Protein sequences were aligned with Clustal Omega (78). The blue shaded residues are
1068 predicted to be extracellular, the transmembrane domain is shaded in grey, and the predicted
1069 NERD domain is shaded in yellow. *S. aureus* NCTC8325-4 is highlighted in bold, and residues
1070 that were mutated are marked in green. The accession numbers of the sequences are indicated,
1071 and the first five letter in the sequence tags indicate the genus or species corresponding the to
1072 the sequences (for example, Nosoc; *Nococomiicoccus*, Aliic; *Aliicoccus*, Salin; *Salinicoccus*,
1073 Jeotg; *Jeotgalicoccus*, Auric; *Auricoccus*, Abyss; *Abyssicoccus*, Mepid; *Macrococcus*
1074 *epidermidis*, Mcase; *Macrococcus caseolyticus*, Ssciu; *Staphylococcus sciuri*, Sinte;
1075 *Staphylococcus intermedius*).

1076

1077 **Fig. S2. Growth of SmdA knockdown strains in liquid cultures and verification of *smdA***
1078 **silencing. (A)** Growth of $SmdA^{down}$ in *S. aureus* SH1000 (IM269) compared to the CRISRPi-
1079 control strain with a non-targeting sgRNA (IM284). IPTG (300 µg/ml) was added to induce
1080 expression of the CRISPRi-system and CFU/ml and OD_{600} measured every hour for five hours.
1081 (**B**) Verification of *smdA* silencing by PCR with RT-PCR. cDNA was synthesized from RNA
1082 isolated from induced and un-induced cultures of SH1000 $SmdA^{down}$ (IM269) and the CRISPRi
1083 control strains (IM284; non-targeting sgRNA and IM165; empty plasmid without sgRNA).
1084 Primers targeting either *smdA* or the housekeeping gene *pta*.

1085

1086 **Fig. S3. Transmission electron microscopy (TEM) of different *S. aureus* strains with**
1087 **SmdA knockdown.** $SmdA^{down}$ and control cells analyzed with TEM in the *S. aureus* strains

1088 (**A**) NCTC8325-4 (IM311 and IM307), (**B**) HG001 (IM312 and IM313) and (**C**) COL (IM294
1089 and IM295). Th e sizes of the scale bars are indicated in the images.
1090
1091 **Fig. S4. Scanning electron microscopy (SEM) of cells depleted of SmdA.** SEM micrographs
1092 of SmdA^{down} and control cells in *S. aureus* (**A**) HG001 (IM312 and IM313) and (**B**) COL
1093 (IM294 and IM295). All scale bars, 1 µm.
1094
1095 **Fig. S5. Overexpression of SmdA.** (**A**) Induced expression of an ectopic copy of *smdA* in the
1096 plasmid pLOW in *S. aureus* NCTC8325-4 (MK1866). Cells were labelled with the cell wall
1097 marker fluorescent vancomycin (VanFL). Scale bar, 2 µm. (**B**) Autolysis of *S. aureus* SmdA
1098 overexpression strain (MK1866) compared to plasmid control strain (MK1465) monitored in
1099 presence of 0.5 % Triton X-100. Results presented as % of initial OD_{600}. Error bars represent
1100 standard error calculated from four technical replicates.
1101
1102 **Fig. S6. Analysis of teichoic acids.** (**A-B**) Lipoteichoic acid (LTA) detection by
1103 immunoblotting with α-LTA antibody was performed with (**A**) cell extract samples from
1104 SmdA^{down} and CRISPRi control cells from *S. aureus* SH1000 (IM269 and IM284),
1105 NCTC8325-4 (IM311 and IM307), HG001 (IM312 and IM313) and COL (IM294 and IM295),
1106 and (**B**) cell extract (CE)- and supernatant (SN) samples from SmdA^{down} and CRISPRi control
1107 cells from *S. aureus* SH1000 and NCTC8325-4 (IM269, IM284, IM311 and IM307,
1108 respectively). In (A), the mean intensities in the bands (background subtracted) were
1109 determined using Fiji (71). The mean intensities of the LTA bands in the *smdA* depletions
1110 relative to their controls are plotted. All control strains express a non-targeting sgRNA. (**C-D**)
1111 SmdA does not have major impact on the synthesis of wall teichoic acids. (**C**) TEM
1112 micrographs of *S. aureus* NCTC8325-4 control strain (IM307) compared to SmdA and TarO

1113 knockdown strains IM311 and IM358, respectively. The black arrows indicate presence of a
1114 high-density layer in the septum, which is missing in the TarO depletion strain (white arrow).
1115 (**D**) Fourier transform infrared spectroscopy (FTIR) of *S. aureus* HG001 control strain (IM313)
1116 and knockdown strain of SmdA and TarO (IM312 and IM357, respectively). The
1117 polysaccharide region of the spectrum is shown, and the indicated peaks represents α- and β-
1118 glycosidic bonds.
1119
1120 **Fig. S7.** Bacterial two-hybrid analysis demonstrating self-interaction between SmdA proteins.
1121 Blue bacterial spots indicate positive interactions and white spots indicate no interaction.
1122
1123 **Table S1. Proteins pulled down with SmdA-GFP.**
1124
1125 **Table S2. Strains used in this study.**
1126
1127 **Table S3. Primers used in this study.**

1128 **Fig. 1**

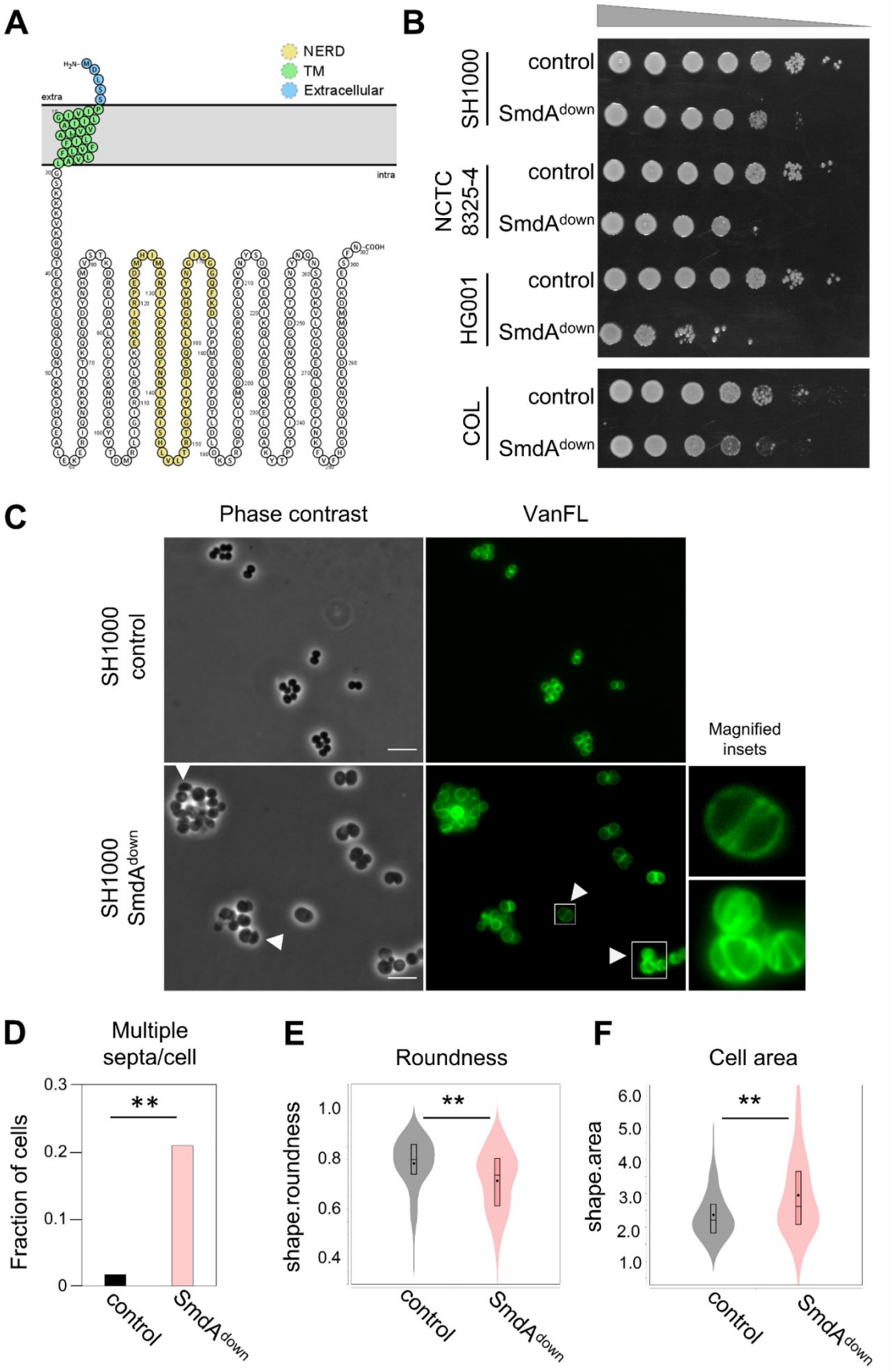

1129

1130 **Fig. 2**

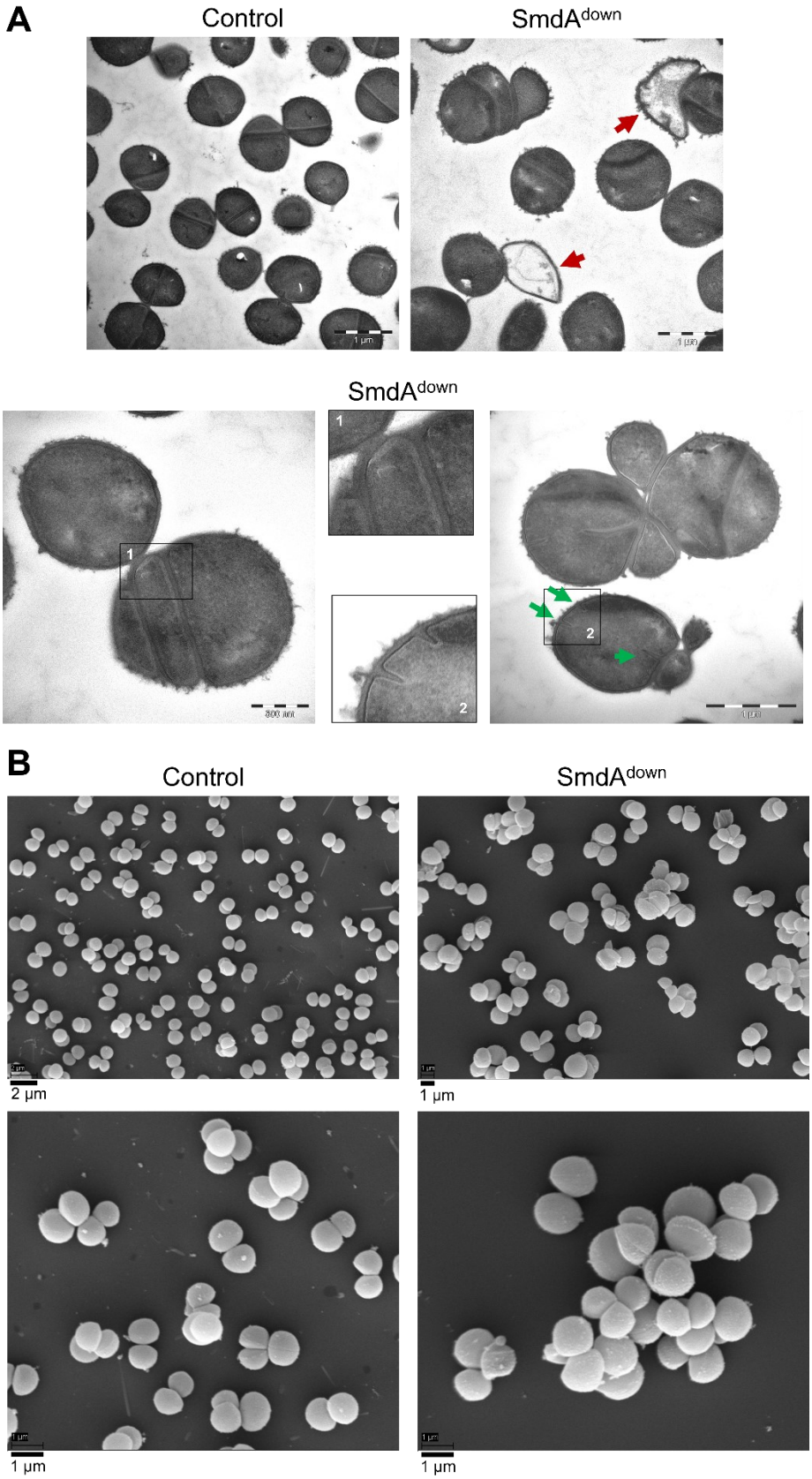

1131

1132

1133 **Fig. 3**

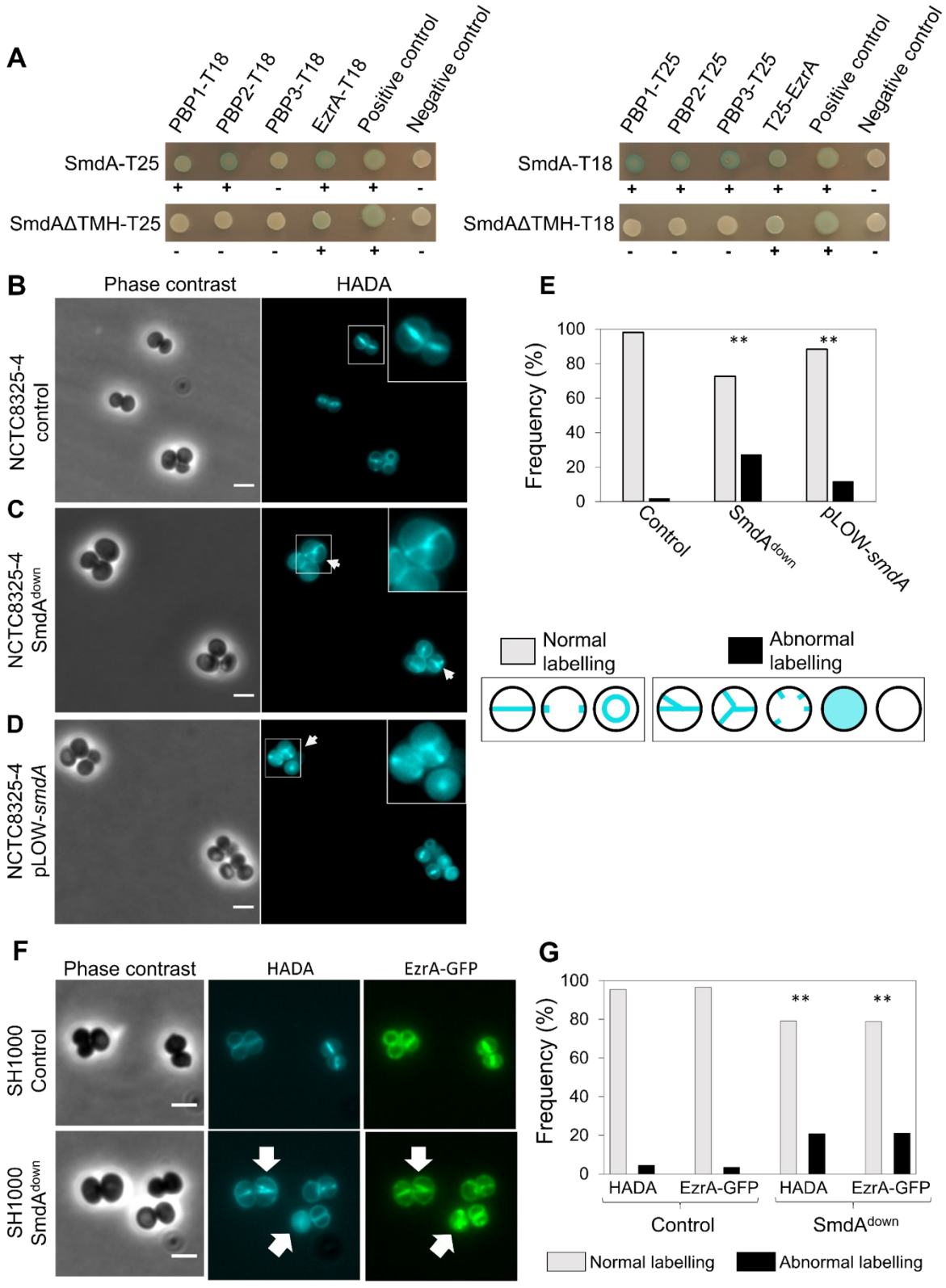

1134

1135

1136 **Fig. 4**

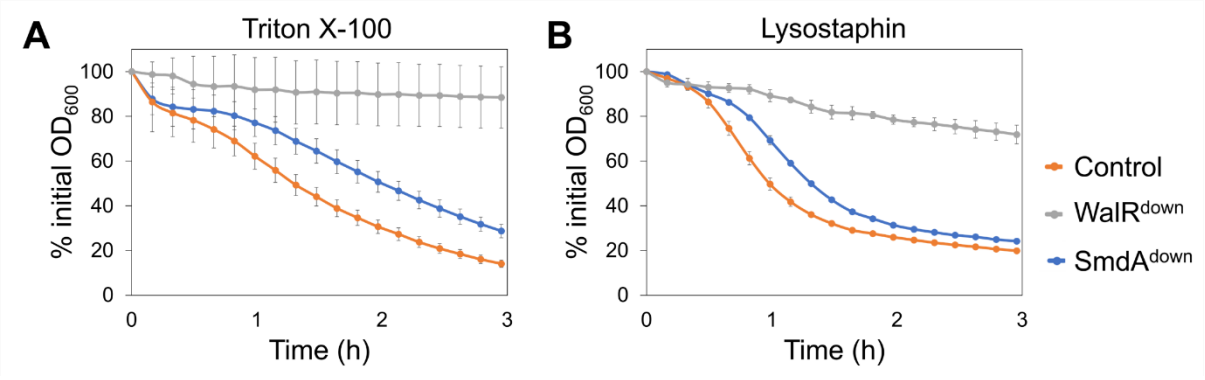

1137

1138 **Fig. 5**

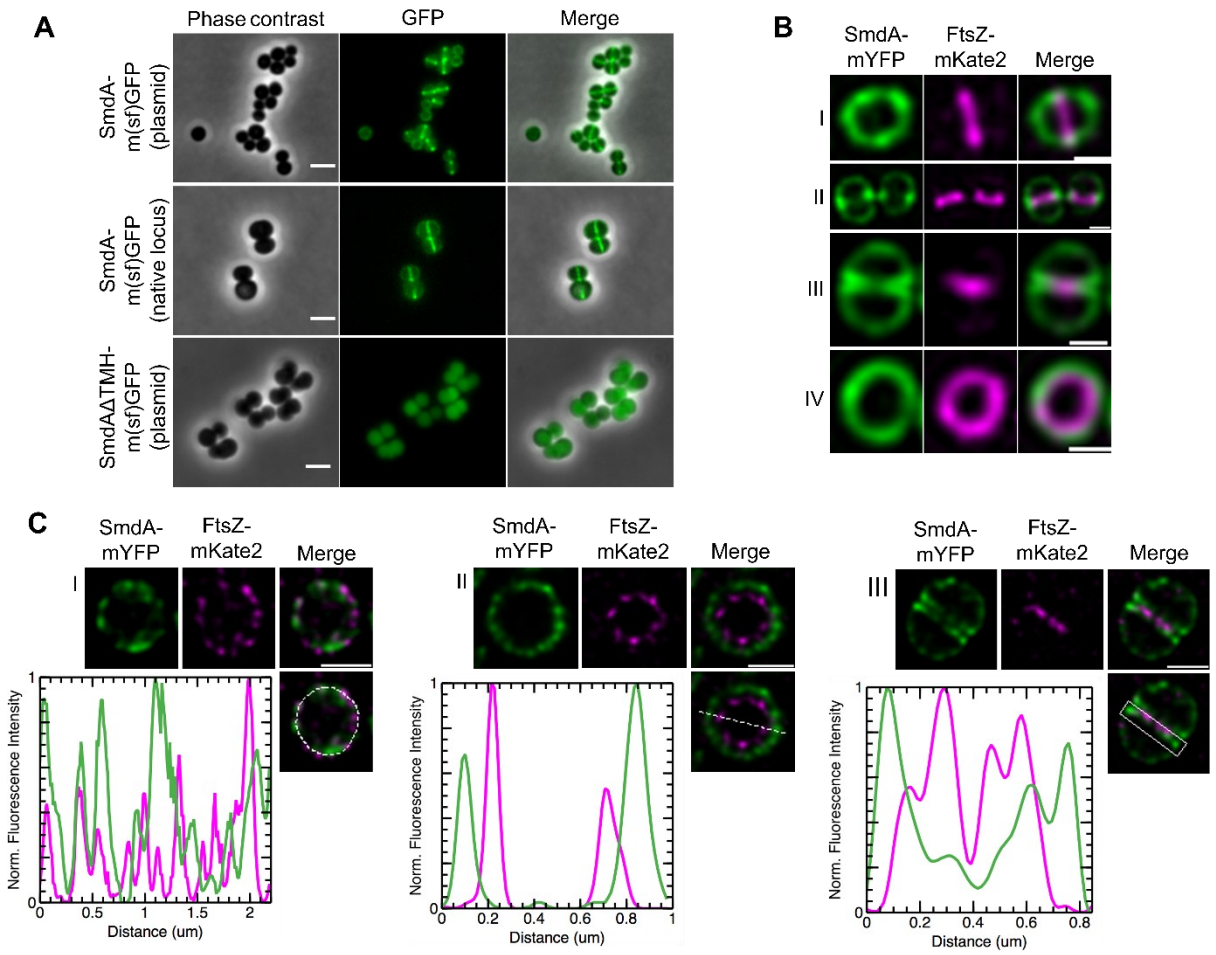

1139

1140

1141 **Fig. 6**

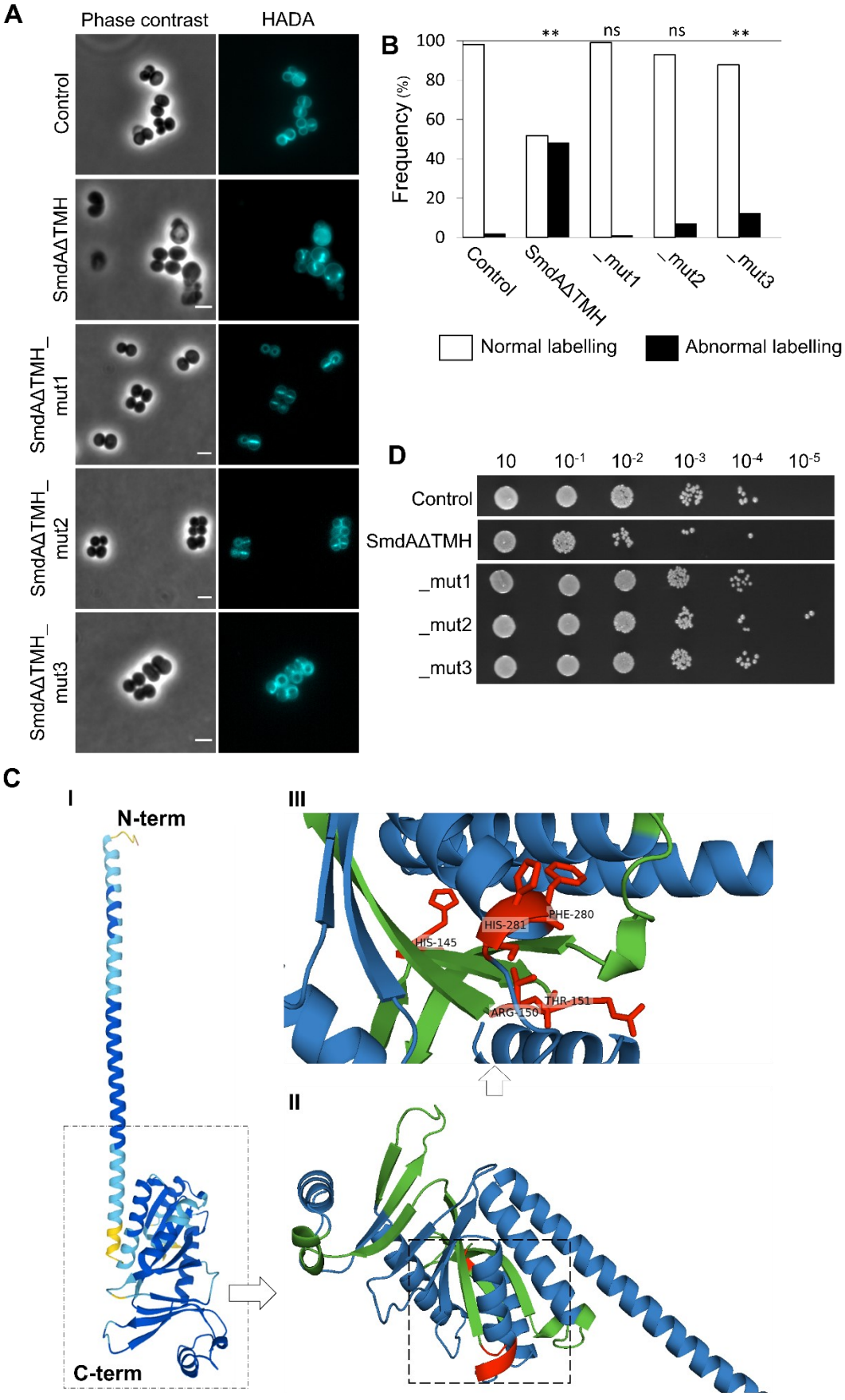

1142